Quantum instanton evaluation of the kinetic isotope effects

Jiří Vaníček* and William H. Miller

Department of Chemistry and Kenneth S. Pitzer Center for Theoretical Chemistry, University of California, Berkeley, CA 94720

Jesús F. Castillo and F. Javier Aoiz

Department of Physical Chemistry and Department of Chemistry, Universidad Complutense de Madrid, Spain

(Dated: April 14, 2005)

Abstract

A general quantum-mechanical method for computing kinetic isotope effects is presented. The method is based on the quantum instanton approximation for the rate constant and on the path integral Metropolis Monte-Carlo evaluation of the Boltzmann operator matrix elements. It computes the kinetic isotope effect directly, using a thermodynamic integration with respect to the mass of the isotope, thus avoiding the more computationally expensive process of computing the individual rate constants. The method is more accurate than variational transition-state theories or the semiclassical instanton method since it does not assume a single reaction path and does not use a semiclassical approximation of the Boltzmann operator. While the general Monte-Carlo implementation makes the method accessible to systems with a large number of atoms, we present numerical results for the Eckart barrier and for the collinear and full three-dimensional isotope variants of the hydrogen exchange reaction $H+H_2 \rightarrow H_2+H$. In all seven test cases, for temperatures between 250 K and 600 K, the error of the quantum instanton approximation for the kinetic isotope effects is less than $\sim$10%.

I. INTRODUCTION

Kinetic isotope effects (KIEs) belong among the main tools of chemical kinetics in determining mechanisms of complex chemical reactions or determining the extent of nuclear quantum mechanical effects in a simple reaction.[1–3] These effects are particularly strong for hydrogen transfer reactions with a high activation barrier or at low temperatures. However, KIEs have been used to show that in some enzymatic reactions, the hydrogen transfer proceeds via tunneling even at room temperature with the help of thermally excited "promoting" vibrations that modulate the donor-acceptance distance.[4–10]

By definition, KIE is the ratio of the rate constants of the lighter and heavier isotopic variants of a chemical reaction, and in general differs from unity due to several different factors. Since the early days of chemical kinetics, KIEs have been mostly described from the perspective of transition state theory (TST).[1,2,11] This theory is intrinsically classical, although various quantum "corrections" have been incorporated in it over time. For instance, observed zero-point-energy effects can be accounted for by replacing classical partition functions by their quantum analogs. For high enough temperature, tunneling can be accounted for by the Wigner correction.[12] For low temperatures, tunneling and accompanying "corner-cutting" can be accounted for by finding optimal tunneling paths.[13–15] Since the very concept of trajectory is ill-defined in quantum mechanics, a tube of trajectories should be considered, which is done, e.g., in the semiclassical instanton method[16,17] that takes these quantum fluctuations into account, at least in the harmonic approximation.

There are various approaches to find exact quantum-mechanical rate constants,[18,19] but in general these are not feasible for systems with many degrees of freedom. One therefore often resorts to various simplifying approximations that make a computation practicable but are less severe than even the improved versions of TST. Among these belongs a variety of quantum transition state theories (QTSTs).[20–32] Another option is to treat only the most important (generally only one or two) degrees of freedom quantum mechanically and the rest classically, as is the case, e.g., in the mixed quantum/classical molecular dynamics with quantum transitions[33] or in the quantum-classical path method with an empirical valence bond potential energy surface.[34]

A recent paper[35] has introduced a new type of QTST, motivated by the semiclassical (SC) instanton model,[16] and is therefore referred to as the quantum instanton (QI) ap-

proximation. The similarity between the quantum and semiclassical instanton theory lies in using the steepest descent approximation to evaluate relevant integrals in the quantum mechanical rate expression, while the critical difference is that the Boltzmann operators in the QI expression are evaluated fully quantum mechanically rather than within the semiclassical approximation. The quantum instanton theory thus incorporates all the tunneling, corner-cutting, and quantum-fluctuations effects correctly and is expected to overcome the quantitative deficiency of the SC instanton model.[36] Indeed, several test applications have shown the QI theory to give accurate quantum rates over a wide temperature range, from the "deep" tunneling regimes at low temperatures to the regime of over-barrier dynamics at high temperature.[35,37–42] A practical path integral Monte-Carlo (PIMC)[43–45] scheme has also been developed to evaluate the QI rate for more complex reactions.[37,38]

While the theoretical KIE is usually computed by finding the absolute rate constants for the isotopic variants first and then calculating their ratio,[15,33,34] it is often much easier experimentally to measure the KIE directly. Similarly, in this paper we describe an efficient procedure, based on the QI approximation, for computing the KIE directly, using a thermodynamic integration[46,47] with respect to the mass of the isotope. Because our method is based on the PIMC integration, it scales favorably with the dimensionality of the system even if all degrees of freedom are treated quantum-mechanically. However, if a different number of imaginary-time slices is used in the discretization of the path integral for each degree of freedom, a virtually continuous choice is possible between a fully classical (one slice) and a fully quantum-mechanical (many slices) treatment of each degree of freedom separately.[42,48] The direct method of computation of KIEs described here is efficient particularly because it avoids umbrella sampling[46] necessary in computing the absolute rate constants.[37,38]

The remainder of this paper is organized as follows: Section II provides a simple covariant (coordinate independent) derivation of the QI expression. Section III shows how the QI theory is applied to the KIEs via the thermodynamic integration. In Sec. IV, we describe the path integral formalism for evaluating the KIEs within the QI approximation. Section V gives an overview of the traditional TST framework for KIEs, in particular the high temperature limit of TST is discussed. Section VI summarizes the exact quantum-mechanical (QM) method (i. e., a quantum reactive scattering calculation) for computing the rate constants of bimolecular reactions A+BC $\rightarrow$ AB+C in three dimensions. This method is used

in the following section to provide a benchmark for evaluating the QI approach. In Sec. VII we numerically test the QI approximation for KIEs from Secs. II-IV and compare it to the exact quantum KIEs and to the high temperature limit of simple TST, for three systems of increasing complexity—for the Eckart barrier and for the collinear as well as full three-dimensional isotopic variants of the H+H_2 → H_2+H reaction. Section VIII summarizes the main conclusions of this paper.

II. QUANTUM INSTANTON APPROXIMATION FOR THE THERMAL RATE CONSTANT

The quantum instanton approximation for thermal rate constants was introduced in Ref. 35 where it was derived from the exact expression

$$kQ_r = (2\pi\hbar)^{-1} \int_0^\infty dE\, N\,(E)\, e^{-\beta E}. \tag{2.1}$$

Here k is the thermal rate constant, Q_r is the reactant partition function, $N(E)$ is the cumulative reaction probability at total energy E, and $\beta = 1/k_B T$ is the inverse temperature. An alternative derivation[49] starts from the exact Miller-Schwartz-Tromp formula,[50]

$$kQ_r = \int_0^\infty dt\, C_{ff}\,(t) \tag{2.2}$$

where $C_{ff}\,(t)$ is the symmetrized (and therefore real) flux-flux correlation function,

$$C_{ff}\,(t) = \mathrm{tr}\left(e^{-\beta\hat{H}/2}\hat{F}_a e^{-\beta\hat{H}/2} e^{i\hat{H}t/\hbar}\hat{F}_b e^{-i\hat{H}t/\hbar}\right) \tag{2.3}$$

with Hamiltonian operator $\hat{H}$, and flux operators $\hat{F}_\gamma$ defined by

$$\hat{F}_\gamma = \frac{i}{\hbar}\left[\hat{H}, h\left[\xi_\gamma\left(\mathbf{r}\right)\right]\right], \tag{2.4}$$

$h\left(\xi_\gamma\right)$ being the Heaviside function. The above equations involve two dividing surfaces, defined by $\xi_\gamma\left(\mathbf{r}\right) = 0$, $\gamma = a, b$; i.e., $\xi_a(\mathbf{r})$ and $\xi_b(\mathbf{r})$ are generalized reaction coordinates, functions of the coordinates $\mathbf{r}$ that take on positive (negative) value on the product (reactant) sides of the dividing surfaces. The quantum instanton expression follows by multiplying and dividing the integrand of Eq.(2.2) by the "delta-delta" correlation function $C_{dd}\,(t)$ and applying the stationary-phase approximation to the resulting integral

$$kQ_r = \int_0^\infty dt\, C_{dd}\,(t)\, \frac{C_{ff}\,(t)}{C_{dd}\,(t)}, \tag{2.5}$$

assuming that $C_{ff}(t)/C_{dd}(t)$ varies slowly compared with $C_{dd}(t)$ and that the stationary-phase point is at $t = 0$. The result is

$$k \approx k_{QI} = \frac{1}{Q_r} C_{ff}(0) \frac{\sqrt{\pi}}{2} \frac{\hbar}{\Delta H} \tag{2.6}$$

where ΔH is a specific type of energy variance,[37]

$$\Delta H = \hbar \left[\frac{-\ddot{C}_{dd}(0)}{2C_{dd}(0)} \right]^{1/2}. \tag{2.7}$$

The delta-delta correlation function used above is defined as

$$C_{dd}(t) = \mathrm{tr}\left(e^{-\beta\hat{H}/2} \hat{\Delta}_a e^{-\beta\hat{H}/2} e^{i\hat{H}t/\hbar} \hat{\Delta}_b e^{-i\hat{H}t/\hbar} \right) \tag{2.8}$$

where the generalized delta function operator is

$$\hat{\Delta}_\gamma = \Delta\left[\xi_\gamma(\hat{\mathbf{r}})\right] \equiv \delta\left[\xi_\gamma(\hat{\mathbf{r}})\right] \left\|\nabla\xi_\gamma\right\|_- \tag{2.9}$$

and the norm of a covariant vector $\nabla\xi_\gamma$ is

$$\left\|\nabla\xi_\gamma\right\|_- = \sqrt{\sum_{i=1}^{N} \frac{1}{m_i} \left|\nabla_i \xi_\gamma(\mathbf{r})\right|^2} \tag{2.10}$$

(the "-" sign subscript on the left-hand side denotes that the negative first power of m_i must be used in the norm of a covariant vector). The two dividing surfaces γ are determined within the QI approximation model by the requirement that $C_{dd}(0)$ be stationary with respect to the change in their location,

$$\frac{\partial C_{dd}}{\partial \eta_k} = 0 \quad \text{for all} \quad k \quad \text{and all} \quad \lambda \in [0,1], \tag{2.11}$$

where $\{\eta_k\}$ is a set of parameters controlling the location of the dividing surfaces. This stationary condition originates from semiclassical considerations of the periodic orbit in imaginary time with period $\hbar\beta$ (i.e., the "instanton"); the two dividing surfaces correspond qualitatively to the location of the turning point surfaces of this periodic orbit.

III. APPLICATION TO THE KINETIC ISOTOPE EFFECTS

The kinetic isotope effect (KIE) is defined as the ratio k_A/k_B of rate constants for two isotopologues A and B. Isotopologues A and B are two chemical species differing only by

replacing an atom (or a group of atoms) in A by its (their) isotope(s) in B. It will turn out below to be convenient to consider the isotope change to be continuous, and parametrized by a real number $\lambda \in [0,1]$, where $\lambda = 0$ for isotopes present in A and $\lambda = 1$ for isotopes in B. Within the Born-Oppenheimer approximation, the potential energy surface (PES) for the reaction does not change, the only change in the Hamiltonian being in the mass of the isotopes. We can therefore define λ by

$$m_i(\lambda) = m_{A,i}(1-\lambda) + m_{B,i}\lambda \tag{3.1}$$

where $m_{A,i}$ and $m_{B,i}$ are the masses of the ith atom in the isotopologues A and B, respectively. Within the quantum instanton approximation (2.6), the KIE can be expressed as

$$\frac{k_0}{k_1} = \frac{Q_{r1}}{Q_{r0}} \times \frac{\Delta H_1}{\Delta H_0} \times \frac{C_{ff}(0)_0}{C_{ff}(0)_1}, \tag{3.2}$$

the numeric subscript denoting the value of λ. The Metropolis path integral Monte-Carlo algorithm that we shall use to evaluate the KIE is only capable of finding normalized quantities, such as $C_{ff}(0)_\lambda / C_{dd}(0)_\lambda$ or $\Delta H_\lambda = \hbar \left[-\ddot{C}_{dd}(0)_\lambda / 2C_{dd}(0)_\lambda \right]^{1/2}$. It therefore pays to rewrite Eq. (3.2) as

$$\frac{k_0}{k_1} = \frac{Q_{r1}}{Q_{r0}} \times \frac{\Delta H_1}{\Delta H_0} \times \frac{C_{dd}(0)_0}{C_{dd}(0)_1} \times \frac{\frac{C_{ff}(0)_0}{C_{dd}(0)_0}}{\frac{C_{ff}(0)_1}{C_{dd}(0)_1}}. \tag{3.3}$$

Ratios $C_{dd}(0)_1 / C_{dd}(0)_0$ and Q_{r1}/Q_{r0} contain quantities with different values of λ and cannot be directly evaluated by the PIMC method. In order to circumvent this obstacle, we use a *thermodynamic integration*[46,47] (also known as the *charging algorithm*) with respect to the parameter λ. While $Q_r(\lambda)$ is not a normalized quantity, its logarithmic derivative, $d \log Q_r(\lambda)/d\lambda = \frac{dQ_r(\lambda)}{d\lambda}/Q_r(\lambda)$, is and can be directly computed by the PIMC method. We can therefore find the ratio of the partition functions, and similarly, delta-delta correlation functions, as

$$\frac{Q_{r1}}{Q_{r0}} = \exp\left[\int_0^1 d\lambda \frac{d \log Q_r(\lambda)}{d\lambda} \right], \tag{3.4}$$

$$\frac{C_{dd}(0)_1}{C_{dd}(0)_0} = \exp\left[\int_0^1 d\lambda \frac{d \log C_{dd}(0)(\lambda)}{d\lambda} \right]. \tag{3.5}$$

IV. PATH INTEGRAL REPRESENTATION OF RELEVANT QUANTITIES

Equations (3.3)-(3.5) contain four types of expressions. As mentioned above, $C_{ff}(0)_\lambda / C_{dd}(0)_\lambda$ and ΔH_λ are directly suitable for Metropolis PIMC evaluation and path-

integral estimators for these quantities have been derived in Refs. 37,38. In our case, we need a generalization of the estimators from the Appendix of Ref. 37. For completeness, this generalization is written out explicitly in Appendix A. Otherwise, we only need to find path-integral expressions for $d\log Q_r\left(\lambda\right)/d\lambda$ and $d\log C_{dd}(0)\left(\lambda\right)/d\lambda$.

We start with the path integral representation for Q_r,

$$Q_r \simeq V^{-2}C\int d\mathbf{r}^{(1)}\int d\mathbf{r}^{(2)}\cdots\int d\mathbf{r}^{(P)}\rho_r\left(\left\{\mathbf{r}^{(s)}\right\}\right), \tag{4.1}$$

$$\rho_r\left(\left\{\mathbf{r}^{(s)}\right\}\right) = \exp\left[-\beta\Phi\left(\left\{\mathbf{r}^{(s)}\right\}\right)\right], \tag{4.2}$$

where V is the volume,[87] $C \equiv \left(\frac{P}{2\pi\hbar^2\beta}\right)^{NdP/2}\prod_{i=1}^{N} m_i^{dP/2}$ is a multiplicative constant, P is the number of imaginary time slices, and $\mathbf{r}^{(s)} \equiv \left(\mathbf{r}_1^{(s)}, \mathbf{r}_2^{(s)}, \ldots, \mathbf{r}_N^{(s)}\right)$ the set of Cartesian coordinates associated with the sth time slice. ρ_r is the thermal density matrix in the reactant region and $\beta\Phi\left(\left\{\mathbf{r}^{(s)}\right\}\right)$ is the discretized "action" given by

$$\Phi\left(\left\{\mathbf{r}^{(s)}\right\}\right) = \frac{P}{2\hbar^2\beta^2}\sum_{s=1}^{P}\sum_{i=1}^{N} m_i\left(\mathbf{r}_i^{(s)} - \mathbf{r}_i^{(s-1)}\right)^2 + \frac{1}{P}\sum_{s=1}^{P} V\left(\mathbf{r}^{(s)}\right) \tag{4.3}$$

with $\mathbf{r}^{(0)} \equiv \mathbf{r}^{(P)}$ and $\left\{\mathbf{r}^{(s)}\right\}$ representing $\left\{\mathbf{r}^{(1)}, \mathbf{r}^{(2)}, \ldots, \mathbf{r}^{(P)}\right\}$. The Monte-Carlo estimator for the logarithmic derivative of Q_r easily follows,

$$\frac{d\log Q_r\left(\lambda\right)}{d\lambda} \simeq \sum_{i=1}^{N}\frac{dm_i}{d\lambda}\left\langle\frac{dP}{2m_i} - \beta\frac{\partial\Phi}{\partial m_i}\right\rangle_{\rho_r}, \tag{4.4}$$

$$\frac{\partial\Phi}{\partial m_i} = \frac{P}{2\hbar^2\beta^2}\sum_{s=1}^{P}\left(\mathbf{r}_i^{(s)} - \mathbf{r}_i^{(s-1)}\right)^2. \tag{4.5}$$

Here $\left\langle A\right\rangle_\rho$ denotes the Monte-Carlo average of quantity A over discretized paths $\left\{\mathbf{r}^{(s)}\right\}$, weighted with a density ρ,

$$\left\langle A\right\rangle_\rho \equiv \frac{\int d\mathbf{r}^{(1)}\int d\mathbf{r}^{(2)}\cdots\int d\mathbf{r}^{(P)} A\left(\left\{\mathbf{r}^{(s)}\right\}\right)\rho\left(\left\{\mathbf{r}^{(s)}\right\}\right)}{\int d\mathbf{r}^{(1)}\int d\mathbf{r}^{(2)}\cdots\int d\mathbf{r}^{(P)}\rho\left(\left\{\mathbf{r}^{(s)}\right\}\right)}. \tag{4.6}$$

$\left\langle A\right\rangle_\rho$ is the PIMC approximation to the QM thermal average of the quantity A, $\mathrm{tr}\,\hat{A}\hat{\rho}/\,\mathrm{tr}\,\hat{\rho}$.

Similarly, the path integral expression for $C_{dd}\left(0\right)$ is

$$C_{dd}\left(0\right) \simeq V^{-1}C\int d\mathbf{r}^{(1)}\int d\mathbf{r}^{(2)}\cdots\int d\mathbf{r}^{(P)}\rho^{\ddagger}\left(\left\{\mathbf{r}^{(s)}\right\}\right), \tag{4.7}$$

$$\rho^{\ddagger}\left(\left\{\mathbf{r}^{(s)}\right\}\right) = \Delta\left[\xi_a\left(\mathbf{r}^{(0)}\right)\right]\Delta\left[\xi_b\left(\mathbf{r}^{(P/2)}\right)\right]\exp\left[-\beta\Phi\left(\left\{\mathbf{r}^{(s)}\right\}\right)\right], \tag{4.8}$$

where $\rho^{\ddagger}$ is the thermal density matrix constrained to the two dividing surfaces ("transition state" region).[88] Since the position of optimal dividing surfaces in general depends on λ, C_{dd} has both an explicit and an implicit dependence on λ, $C_{dd} \equiv C_{dd}(\lambda, \{\eta_k(\lambda)\})$ where $\{\eta_k(\lambda)\}$ is a set of parameters controlling the position of the dividing surfaces. Consequently

$$\frac{dC_{dd}}{d\lambda} = \frac{\partial C_{dd}}{\partial \lambda} + \sum_k \frac{\partial C_{dd}}{\partial \eta_k} \frac{d\eta_k}{d\lambda}, \tag{4.9}$$

where from now on we omit the argument $t = 0$ of C_{dd}. Because of the appearance of extra terms besides $\partial C_{dd}/\partial\lambda$ it seems at first that the thermodynamic integration for C_{dd} would be much more difficult than that for Q_r. However, due to the stationary property (2.11) of the dividing surfaces, we have

$$dC_{dd}/d\lambda = \partial C_{dd}/\partial\lambda. \tag{4.10}$$

The estimator for the logarithmic derivative is therefore

$$\frac{d\log C_{dd}}{d\lambda} \simeq \sum_{i=1}^{N} \frac{dm_i}{d\lambda} \left\langle \frac{dP}{2m_i} - \beta \frac{\partial \Phi}{\partial m_i} - \sum_{\gamma=a,b} \frac{|\nabla_i \xi_\gamma|^2}{2m_i^2 \left\|\nabla \xi_\gamma\right\|_-^2} \right\rangle_{\rho^{\ddagger}}, \tag{4.11}$$

where ξ_a is evaluated at $\mathbf{r}^{(0)}$ and ξ_b at $\mathbf{r}^{(P/2)}$.

For numerical computation we used a generalization of the Gaussian approximation of the delta function from Ref. 37,

$$\tilde{\delta}\left[\xi\left(\mathbf{r}\right)\right] \equiv \left(\frac{2P}{\pi\hbar^2\beta}\right)^{1/2} \frac{1}{\left\|\nabla\xi\right\|_-} \exp\left\{-\frac{2P}{\hbar^2\beta}\left[\frac{\xi\left(\mathbf{r}\right)}{\left\|\nabla\xi_\gamma\right\|_-}\right]_-^2\right\}, \tag{4.12}$$

$$\tilde{\Delta}\left[\xi\left(\mathbf{r}\right)\right] = \left(\frac{2P}{\pi\hbar^2\beta}\right)^{1/2} \exp\left\{-\frac{2P}{\hbar^2\beta}\left[\frac{\xi\left(\mathbf{r}\right)}{\left\|\nabla\xi_\gamma\right\|_-}\right]^2\right\}.$$

With this approximation, estimators for all quantities constrained to the dividing surfaces must have ξ_a evaluated at $\bar{\mathbf{r}}^{(1)}$ instead of $\mathbf{r}^{(0)}$ and ξ_b at $\bar{\mathbf{r}}^{(P/2+1)}$ instead of $\mathbf{r}^{(P/2)}$, where $\bar{\mathbf{r}}^{(s)} = \frac{1}{2}\left(\mathbf{r}^{(s)} + \mathbf{r}^{(s-1)}\right)$ (see Ref. 37 for explanation). The constrained density matrix $\rho^{\ddagger}$ as well as the estimators for $C_{ff}\left(0\right)/C_{dd}\left(0\right)$ and ΔH must be adjusted in a similar manner as in Ref. 37. See Appendix A for details. Also, the estimator (4.11) for the logarithmic derivative of C_{dd} changes and becomes

$$\frac{d\log C_{dd}}{d\lambda} \simeq \sum_{i=1}^{N} \frac{dm_i}{d\lambda} \left\langle \frac{dP}{2m_i} - \beta \frac{\partial \Phi}{\partial m_i} - \frac{2P}{\hbar^2\beta} \sum_{\gamma=a,b} \frac{\xi_\gamma^2 \left|\nabla_i \xi_\gamma\right|^2}{m_i^2 \left\|\nabla \xi_\gamma\right\|_-^4} \right\rangle_{\rho^{\ddagger}}, \tag{4.13}$$

$$\rho^{\ddagger}\left(\left\{\mathbf{r}^{(s)}\right\}\right) = \Delta\left[\xi_a\left(\bar{\mathbf{r}}^{(1)}\right)\right] \Delta\left[\xi_b\left(\bar{\mathbf{r}}^{(P/2+1)}\right)\right] \exp\left[-\beta\Phi\left(\left\{\mathbf{r}^{(s)}\right\}\right)\right]. \tag{4.14}$$

V. TRANSITION STATE THEORY FRAMEWORK FOR THE KINETIC ISOTOPE EFFECTS

The quantum-instanton approach described above is capable of capturing such quantum effects as tunneling, "corner-cutting," and anharmonic fluctuations about the semiclassical path, and therefore goes far beyond the capabilities of the conventional transition state theory (TST). Still, before we discuss the numerical results, it is useful to consider KIEs in the framework of TST[1,2,11] because this theory provides a way of classifying various contributions to the KIEs, it is still widely used for describing experimental KIEs, and in fact, it gives quantitative results at least at high enough temperatures (but not so high that recrossing effects become important).

Within transition state theory, the reaction rate is

$$k_{\mathrm{TST}} = \kappa \frac{k_B T}{h} \frac{Q^{\ddagger}}{Q_r} e^{-E_b/k_B T}, \tag{5.1}$$

where κ is the transmission coefficient, $Q^{\ddagger}$ is the partition function of the activated complex (i. e., excluding the unstable motion along the reaction coordinate), and E_b is the classical barrier height. The KIE becomes

$$r_{\mathrm{TST}} = \frac{k_{\mathrm{TST}}\left(\lambda=0\right)}{k_{\mathrm{TST}}\left(\lambda=1\right)} = \frac{\kappa\left(0\right)}{\kappa\left(1\right)} \frac{Q^{\ddagger}\left(0\right)}{Q^{\ddagger}\left(1\right)} \frac{Q_r\left(1\right)}{Q_r\left(0\right)}. \tag{5.2}$$

Assuming approximate separability of the Hamiltonian, the partition function can be factored into translational, rotational, and vibrational components as

$$Q = Q_{\mathrm{trans}} \times Q_{\mathrm{rot}} \times Q_{\mathrm{vib}}.$$

At high temperature, we may use the classical forms of the three components of the partition function,

$$Q_{\mathrm{trans}} = (2\pi m k_B T/h^2)^{d/2}, \tag{5.3}$$

$$Q_{\mathrm{rot}} = 8\pi^2 (8\pi^3 I_x I_y I_z)^{1/2} (k_B T)^{3/2} \text{ (in 3 dimensions)}, \tag{5.4}$$

$$Q_{\mathrm{vib}} = \frac{k_B T}{\hbar\omega} \text{ (per degree of freedom)}, \tag{5.5}$$

where I_x, I_y, I_z are the moments of inertia along the principal axes and ω is the angular frequency of the vibration. The TST expression (5.2) greatly simplifies if we further use the

Teller-Redlich product theorem.[51,52] For the most general case of a nonlinear molecule in three dimensions, this theorem reads,

$$\left[\frac{m(0)}{m(1)}\right]^{3/2}\left(\frac{I_{x0}I_{y0}I_{z0}}{I_{x1}I_{y1}I_{z1}}\right)^{1/2}=\prod_{i=1}^{N}\frac{m_i(0)}{m_i(1)}\prod_{j=1}^{3N-6}\frac{\omega_j(0)}{\omega_j(1)} \tag{5.6}$$

where $m=\sum_{i=1}^{N}m_i$ is the total mass of the molecule and ω_j is the angular frequency of the jth normal mode. After substitution into Eq. (5.2) we obtain the classical (or infinite temperature) limit of the KIE, which is temperature-independent,

$$r_{\text{class}}=\frac{s^{\ddagger}(1)}{s^{\ddagger}(0)}\frac{s_r(0)}{s_r(1)}\frac{|\omega^{\ddagger}_{\text{unst}}(0)|}{|\omega^{\ddagger}_{\text{unst}}(1)|}. \tag{5.7}$$

Here $s^{\ddagger}$ and s_r are the symmetry factors for the transition state and reactants, respectively, and $\omega^{\ddagger}_{\text{unst}}$ is the (imaginary) frequency for the unstable "vibration" along the reaction coordinate at the transition state.

The first correction to the transmission coefficient at high but finite temperatures is the order $1/T^2$ expansion of the Wigner tunneling correction,

$$\kappa=1+\frac{1}{24}\left(\hbar\left|\omega^{\ddagger}_{\text{unst}}\right|/k_BT\right)^2,$$

Similar corrections appear for the partition functions for all vibrational degrees of freedom,

$$\frac{Q^{\text{QM}}_{\text{vib}}}{Q^{\text{class}}_{\text{vib}}}=\frac{\hbar\omega/k_BT}{2\sinh\left(\hbar\omega/2k_BT\right)}\approx 1-\frac{1}{24}\left(\frac{\hbar\omega}{k_BT}\right)^2+O\left(T^{-3}\right).$$

Including these corrections in the high temperature limit, the kinetic isotope ratio becomes

$$r_{\text{high }T}=r_{\text{class}}\left\{1+\frac{1}{24}\left(\frac{\hbar}{k_BT}\right)^2\left[\Omega(0)^2-\Omega(1)^2\right]\right\}, \tag{5.8}$$

$$\Omega(\lambda)^2\equiv\sum_j\omega_{r,j}(\lambda)^2-\sum_{j'}\omega^{\ddagger}_{j'}(\lambda)^2,$$

where $\omega_{r,j}$ and $\omega^{\ddagger}_{j'}$ are vibrational (or bending) frequencies of the reactant and the transition state, respectively.

VI. EXACT QUANTUM MECHANICAL METHOD

In order to evaluate the accuracy of the QI approximation for the KIE in the following section, we need an exact benchmark. We will see that for the Eckart barrier, there is an

analytical expression for the cumulative reaction probability (CRP) $N(E)$ from Eq. (2.1). For the collinear reactions, we will use exact results from Refs. 53–56. For the isotopic variants of the full three-dimensional H+H_2 reaction, we carried out our own extensive QM calculations that we describe in this section.

The methodology of these calculations is based on the accurate determination of the cumulative reaction probabilities which has been described extensively in the literature,[57–59] thus only a brief sketch will be given in this section along with the details of the specific calculations.

The thermal rate coefficient $k(T)$ can be written as

$$k(T) = \sum_{J=0} (2J+1) k^J(T), \tag{6.1}$$

where the specific rate constant for total angular momentum J for a bimolecular A+BC reaction, $k^J(T)$, can be written as

$$k^J(T) = \frac{Z_{\rm elec}(T) \int_0^\infty dE \; N^J(E) \; e^{-E/k_B T}}{h \Phi_{\rm rel}(T) Q_{\rm int}^{\rm BC}(T)} \tag{6.2}$$

In Eq. (6.2), $Q_{\rm int}^{\rm BC}(T)$ is the coupled nuclear–rovibrational partition function of BC and $\Phi_{\rm rel}(T)$ is the relative A, BC translational partition function per unit volume. $Z_{\rm elec}(T)$ is the ratio of the electronic partition functions of the transition state and of the atom A. The key quantity in Eq. (6.2) is the total cumulative reaction probability, $N^J(E)$, given by

$$N^J(E) = \sum_{vjK} \sum_{v'j'K'} P^J_{vjK \to v'j'K'}(E) = \sum_{\alpha' \neq \alpha} \sum_{vjK} \sum_{v'j'K'} |S^J_{\alpha' v'j'K',\; \alpha vjK}|^2, \tag{6.3}$$

where $P^J_{vjK \to v'j'K'}(E)$ is the reaction probability from reactants with initial vibrational, rotational, and helicity quantum numbers v, j, K to products with final vibrational, rotational and helicity quantum numbers v', j', K', and α' labels the AC+B, AB+C product arrangement and α the A+BC reagent arrangement.

In the present work, the CRPs have been calculated for all J up to J_{max}, including all the projections in K and K' up to maximum values of $K = \min(J, j, K_{\rm max})$ and $K' = \min(J, j', K_{\rm max})$, where $K_{\rm max}$ have been chosen such that for the highest energy calculated for a given isotopic variant of the reaction contributions from higher K (K') are practically negligible.

The QM reactive scattering matrix has been calculated using a coupled–channel hyperspherical coordinate method of Skouteries *et al.*,[60] which has been employed previously in scattering calculations for the F+H_2,[61–63] F+HD,[64], H+D_2,[65,66] and O(^3P)+HCl[67] reactions. Converged reaction probabilities and CRPs have been calculated at total angular momenta J=0–35 for the H+p–H_2 reaction on the Boothroyd-Keogh-Martin-Peterson (BKMP2) PES[68,69] using a basis set including all H+p–H_2 and HH+H channels with diatomic energy levels up to $E_{\max} = 2.6$ eV and rotational quantum numbers up to $j_{\max} = 15$. Calculations have been carried out for a total of 70 energies between 0.271 eV and 1.651 eV for this isotopic variant. For the D+p–D_2 reaction the CRPs were calculated for J=0–38 using a basis set with $E_{\max} = 2.6$ eV and $j_{\max} = 15$. Note that only reactions with p–H_2 have been considered because the results for p–H_2 and o–H_2 are practically identical. It must be stressed that this is the only approximation used, and that the CRPs have been calculated for all partial waves $J \in [0, J_{\max}]$. For the H+HD reaction the CRPs were calculated for J=0–28 using a basis set with $E_{\max} = 2.6$ eV and $j_{\max} = 16$. Using these basis sets, it has been found that the CRPs are converged to better than 1% for J=0. For $J > 0$, angular basis functions with helicities up to $K_{\max}$=7 for the reactant and product arrangements have been retained *for all the reactions considered*. We have checked that for J=12 the CRPs are converged to 1.0% at the highest energy with the present parameters. The size of the basis sets employed in these calculations is given in Table I.

VII. NUMERICAL RESULTS AND DISCUSSION

We now apply the general procedure for evaluating the KIEs within the QI approximation, described in Sections III and IV, to three systems of increasing complexity: a one-dimensional Eckart barrier, a collinear atom-diatom reaction, and a full three-dimensional atom-diatom reaction A+BC → AB+C. In all three cases, we use parameters corresponding to the H+H_2 reaction and its isotope variants. While the whole computational procedure described in Secs. III and IV is more accurate for two separate dividing surfaces, it has been shown that the error introduced by considering a single dividing surface ($\xi_a = \xi_b = \xi$) is small except at very low temperatures (below $\sim$ 250 K for a D+H_2 reaction).[37] In fact, two independent dividing surfaces actually coalesce into one above 300 K. We therefore use a single dividing surface ξ for numerical calculations. Let us assume that the $\mathbf{r}$ and λ dependence

in the function $\xi(\mathbf{r}, \lambda)$, defining the dividing surface, can be separated,

$$\xi\left(\mathbf{r}, \lambda\right) = \zeta\left(\mathbf{r}\right) - \eta\left(\lambda\right), \tag{7.1}$$

i.e., that there is the same family of dividing surfaces for all isotope variants of the underlying reaction. Which member of this family is used depends on the isotope, and is specified by the parameter $\eta(\lambda)$. Since all systems have an underlying symmetric potential, we could and did choose a function ζ odd under the interchange of atoms A and C (odd under the inversion $x \to -x$ in the case of the Eckart barrier). Namely, for the Eckart barrier we chose $\zeta(x) = x$, and for the A+BC $\to$ AB+C reaction, we chose $\zeta = r_{\mathrm{BC}} - r_{\mathrm{AB}}$, where r_{AB} denotes the distance of atoms A and B.[89] In all computations, we started from a symmetric isotope variant H+H_2 for $\lambda = 0$, and chose $\eta(\lambda = 0) = 0$ because of the symmetry. In cases with symmetric isotopic reaction for $\lambda = 1$ (i.e., H+DH or D+D_2), the symmetry is preserved and so we kept $\eta(\lambda) = 0$. For the asymmetric isotopic reactions for $\lambda = 1$ (i.e., D+H_2 or H+D_2), we evolved the dividing surface position $\eta(\lambda)$ according to the prescription derived in Appendix B.

The Metropolis Monte Carlo sampling was performed with the staging algorithm.[70–72] Besides the staging multiple-slice moves, less frequent single-slice and whole chain moves were used to speed up the exploration of accessible configuration space. Single slice moves were applied specifically to the slices involved in the reaction coordinate (i. e., $\mathbf{r}^{(0)}$, $\mathbf{r}^{(1)}$, $\mathbf{r}^{(P/2)}$, $\mathbf{r}^{(P/2+1)}$) because of the increased rigidity due to the constraint potential.

Each computation was performed with three different numbers of time slices, e. g., $P = 8$, 12, and 16 for $T = 1000$ K. For other temperatures, P was chosen such that $P \times T$ was approximately constant. For each P, the following quantities were computed using the estimators from Sec. IV and Appendix A: $C_{ff}(0)_\lambda / C_{dd}(0)_\lambda$ from Eq. (A1) and ΔH_λ from Eq. (A2), both for $\lambda = 0$ and $\lambda = 1$, $d \log Q_r / d\lambda$ from Eq. (4.4) and $d \log C_{dd} / d\lambda$ from Eq. (4.13), both for several equally spaced values of λ between 0 and 1. Ratios of partition functions and delta-delta correlation functions were then computed using the thermodynamic integration according to Eqs. (3.4) and (3.5). In all cases, it was found that discretizing the change of λ from 0 to 1 in 10 steps was enough to converge the thermodynamic integrals.

For each P, the number of samples was chosen such that the QI result for the KIE had a statistical error below 1%. While the results of the computation with the largest value of P had already a very small discretization error, we extrapolated the values of $C_{ff}(0)_\lambda / C_{dd}(0)_\lambda$,

ΔH_λ, $d\log Q_r/d\lambda$, and $d\log C_{dd}/d\lambda$ for the three values of P up to $P \to \infty$, assuming a discretization error $\propto P^{-2}$. These extrapolated results were used for the calculation of the QI value of the KIE, using Eq. (3.3). This value of the KIE had the combined statistical and extrapolation error always below 1.5% and it is the value that was used in the figures and tables below.

The tables with results also show two other variations of the QI approximation. The so-called "simplest quantum instanton" (SQI) approximation,[49] is

$$k_{\mathrm{SQI}} = \frac{\sqrt{\pi}}{2}\hbar\frac{C_{dd}(0)}{Q_r}, \tag{7.2}$$

and is expected to be accurate only at higher temperatures, compared to the QI result from Eq. (2.6). The "modified QI" (QI-mod),[49] is the QI result augmented by an *ad hoc* correction

$$\Delta H_{\mathrm{mod}}(\beta) = \Delta H(\beta) + \frac{\sqrt{\pi}-\sqrt{2}}{\beta} \tag{7.3}$$

to correct the high temperature (free particle) behavior of the QI. This modified version can significantly improve the QI approximation for the absolute rate, but (as we will see below) not the KIEs in which the errors due to high temperature (free particle) behavior almost completely cancel. (However, the modified QI cannot correct for recrossing effects.)

A. Eckart barrier

The simplest, one-dimensional model, uses the Eckart potential,

$$V(x) = V_0/\cosh(ax)^2, \tag{7.4}$$

with parameters $V_0 = 0.425$ eV and $a = 1.36$ a.u. The mass changes from $m_0 = 1060$ a.u. to $m_1 = 2120$ a.u.[90] In this model, a single translational motion of the reactant becomes an unstable vibration of the transition state. The high temperature limit (5.8) of the KIE gives

$$r_{\mathrm{high}\ T} = \sqrt{\frac{m_1}{m_0}}\left[1 + \frac{1}{24}\left(\frac{\hbar}{k_B T}\right)^2 \left|k^\ddagger_{\mathrm{unst}}\right| \left(\frac{1}{m_0}-\frac{1}{m_1}\right)\right], \tag{7.5}$$

$$k^\ddagger_{\mathrm{unst}} = -\left.\frac{d^2V}{dx^2}\right|_{x=0} = -4V_0a^2,$$

where $k^\ddagger_{\mathrm{unst}}$ is the (negative) force constant at the transition state. In particular, the classical limit (5.7) is $r_{\mathrm{class}} = \sqrt{2} \approx 1.414$.

The exact rate constant for this reaction can be obtained from expression (2.1). In one dimension the cumulative reaction probability equals the transmission probability, which can be derived analytically for the Eckart barrier,

$$\frac{1}{N_{\mathrm{QM}}(E)} = 1 + \frac{\cosh^2\left(\frac{1}{2}\pi\sqrt{8mV_0/\hbar^2a^2 - 1}\right)}{\sinh^2(\pi k/a)}, \tag{7.6}$$

$$k = \sqrt{2mE}/\hbar. \tag{7.7}$$

Figure 1 and Table II show the kinetic isotope effect k_H/k_D for temperatures 100 K to 2400 K, calculated exactly and by various approximations. It is clear that for high temperatures, the exact KIE approaches the parabola representing the high temperature limit (7.5) of TST. QI result follows the exact KIE closely for all temperatures. In particular, for temperatures 300 K and higher, the error of the QI result is within 5%. At low temperatures (200 K and lower), the error of our single-dividing-surface QI increases, which is expected, since there we should correctly use two separate dividing surfaces.[37,49] One of the reasons for the excellent agreement of the QI with exact results at temperatures 300 K and higher is that for systems with one degree of freedom, there is strictly no classical recrossing. Every classical trajectory crosses the top of the barrier at most once. Since the classical TST yields the exact *classical* rates correctly, the only possible errors are of quantum nature and those are well accounted for by the QI approximation.

The modified QI (QI-mod) result (7.3) does not yield a significant improvement over the QI result (3.3). This is so because the QI expression for the rate constant (2.6) underestimates the infinite-temperature free-particle limit for both isotopologues by the same relative error.[49] The "simplest" QI expression (SQI), which is not expected to work for a single dividing surface in its basic form (7.2), gives surprisingly accurate results for temperatures above 300 K. The behavior of the SQI and modified QI approximations for other KIEs described below is similar, we therefore omit this discussion there.

B. Collinear reaction H+H_2 → H_2+H

Our second simplest system is the collinear hydrogen exchange reaction H+H_2 → H_2+H and its isotope variants, D+D_2 → D_2+D, H+DH → HD+H, D+H_2 → DH+H, and H+D_2 → HD+D, on the Truhlar-Kuppermann (TK) potential surface.[53,73] While we could subtract

the center-of-mass motion and make this system effectively two-dimensional, we do not make this simplification and instead treat the model as a system with three degrees of freedom. (The reason is that in future applications of the present PIMC procedure to systems with many degrees of freedom, subtracting the center of mass motion—three degrees of freedom in three spatial dimensions—would not significantly simplify the calculation.) In the collinear case, two translational and one vibrational motion of the reactants turn into a translational, a symmetric (stable) and an asymmetric (unstable) vibration of the transition state. The high temperature limit (5.8) becomes

$$r_{\text{high } T} = \left|\frac{\omega^{\ddagger}_{\text{asym}}(0)}{\omega^{\ddagger}_{\text{asym}}(1)}\right| \left\{1 + \frac{1}{24}\left(\frac{\hbar}{k_B T}\right)^2 \left[\Omega^2_{\text{coll}}(0) - \Omega^2_{\text{coll}}(1)\right]\right\}, \tag{7.8}$$

$$\Omega^2_{\text{coll}}(\lambda) = \frac{k_r}{\mu_{\text{BC}}(\lambda)} + \frac{\left|k^{\ddagger}_{\text{asym}}\right|}{\mu_{\text{AC,B}}(\lambda)} - \frac{k^{\ddagger}_{\text{sym}}}{\mu_{\text{AC}}(\lambda)},$$

where k_r, $k^{\ddagger}_{\text{asym}}$, $k^{\ddagger}_{\text{sym}}$ are force constants of the reactant vibration, of the asymmetric and symmetric vibration of the transition state, respectively. The corresponding reduced masses are $\mu_{\text{BC}} = m_{\text{B}} m_{\text{C}}/(m_{\text{B}} + m_{\text{C}})$, $\mu_{\text{AC,B}} = (m_{\text{A}} + m_{\text{C}}) m_{\text{B}}/(m_{\text{A}} + m_{\text{B}} + m_{\text{C}})$, and $\mu_{\text{AC}} = m_{\text{A}} m_{\text{C}}/(m_{\text{A}} + m_{\text{C}})$. Expression (7.8) works even for asymmetric reactions (D+H_2 and H+D_2), for which the normal mode coordinates differ from the Jacobi coordinates. Expression (7.8) is still true because Ω^2_{coll} is a trace of a certain matrix ($M^{-1/2} K M^{-1/2}$) and therefore is independent of the coordinate system. (M and K are the mass and force constant matrices.) For the TK potential, the values of the force constants are $k_r = 0.3804$ a.u., $k^{\ddagger}_{\text{asym}} = -0.0543$ a.u., $k^{\ddagger}_{\text{sym}} = 0.0782$ a.u. (These are the the force constants corresponding to the non-scaled normal mode coordinates. Often in literature, the transition state force constants are specified for the normal coordinates scaled to the mass of the asymmetric stretch, which would in our case result in a change $k^{\ddagger}_{\text{sym}} \to k^{\ddagger}_{\text{sym}} \times (4/3) \approx 0.1043$ a.u.) In order to find $r_{\text{class}} = |\omega^{\ddagger}_{\text{asym}}(0)/\omega^{\ddagger}_{\text{asym}}(1)|$, in general we need to diagonalize a 2×2 matrix $M^{-1/2} K M^{-1/2}$. Specifically, r_{class}(H+H_2 / D+H_2) ≈ 1.054 and r_{class}(H+H_2 / H+D_2) ≈ 1.332. For the symmetric reactions (H+H_2, D+D_2, and H+DH $\to$ HD+H), the symmetric and asymmetric stretch normal coordinates are the same as the corresponding Jacobi coordinates. For these reactions, the classical limit is particularly simple,

$$r_{\text{class}} = \sqrt{\frac{\mu_{\text{AC,B}}(1)}{\mu_{\text{AC,B}}(0)}}. \tag{7.9}$$

Specifically, $r_{\rm class}(\mathrm{H{+}H_2}\ /\ \mathrm{D{+}D_2}) = \sqrt{2} \approx 1.414$ and $r_{\rm class}(\mathrm{H{+}H_2}\ /\ \mathrm{H{+}DH}) = \sqrt{3/2} \approx 1.225$.

The kinetic isotope effect $k(\mathrm{H{+}H_2})\ /\ k(\mathrm{D{+}D_2})$ in the temperature range 200 to 1500 K is displayed in Fig. 2(a) and Table III. The quantum-mechanical (QM) results are taken from Refs. 53–56 and are said to be accurate to within 2% or better.[53] Again, the figure shows that at high temperatures, the exact KIE approaches the parabola representing Eq. (7.8). For temperatures 300 K and higher, the QI result gives an error within 7%. These results are surprisingly accurate even at high temperatures, considering the dynamical recrossing that is by definition not captured by any (even quantum) transition state theory.

Since dynamical recrossing at high temperatures is a classical effect, its importance at a given energy can be estimated by running classical trajectories and computing the reaction probability defined as

$$P(E) = F_{\rm react}(E)/F_{\rm inc}(E) \tag{7.10}$$

where $F_{\rm react}(E)$ and $F_{\rm inc}(E)$ are the reactive and incident flux, respectively. In Ref. 74, it was found that $P(E)$ computed by TST is essentially exact up to energies 0.2 eV above the barrier, but at energies 1.0 eV, TST overestimates $P(E)$ by a factor of more than 2. In order to estimate the importance of recrossing for the thermal rate constant at a fixed temperature rather than energy, we can use formula (2.1) with $N(E) = P(E)F_{\rm inc}(E)$. Using results from Ref. 74, we estimated the error of the thermal rate constant due to classical recrossing to be less than 1% up to 600 K, 3% at 1000 K and 9% at 1500 K. Presumably, the error of the KIE should be somewhat less than this due to cancellation since recrossing always (i. e., for both isotopologues) results in an overestimation of the rate constant. Bearing in mind this estimate, the error of the QI calculation of the KIE at 1500 K (-5%) is very reasonable. It is neither worse nor (suspiciously) better than what we could expect from the best theory neglecting classical recrossing.

Analogous results for the kinetic isotope effects $k(\mathrm{H{+}H_2})\ /\ k(\mathrm{H{+}DH})$, $k(\mathrm{H{+}H_2})\ /\ k(\mathrm{D{+}H_2})$, and $k(\mathrm{H{+}H_2})\ /\ k(\mathrm{H{+}D_2})$ are displayed in Figs. 2(b)-(d) and Tables IV-VI. Even for the asymmetric reactions, QI results are extremely accurate (within ∼10% error for 300 to 1000 K). The larger error at 200 K for $\mathrm{H{+}D_2}$ is due to the use of a single dividing surface, and at 1500 K due to neglecting the recrossing effects. The reason why the errors for the asymmetric reactions are slightly higher than the errors for the symmetric reactions is

most likely because we varied the dividing surface so that it is stationary only with respect to translations and not rotations (see Appendix B). In particular, the QI approximation correctly captures the temperature behavior of the KIE $k(\mathrm{H+H_2})$ / $k(\mathrm{D+H_2})$ [see Fig. 2(c)] which is inverted compared to the other three KIEs. This unusual behavior is due to the fact that the reactant vibrational partition functions are identical for the two isotopic species and cancel exactly in the KIE. We can see it already in the high T expansion of the TST: The dominant term in expression (7.8) for Ω^2_{coll} is the term $-k_{\mathrm{sym}}/\mu_{\mathrm{AC}}$ and results in the concave dependence of KIE on $1/T$ at high temperatures. For the three other KIEs, the term k_r/μ_{BC} in expression (7.8) for Ω^2_{coll} is dominant and determines the convexity of the high temperature behavior of KIEs.

C. Reaction H+H_2 → H_2+H in three spatial dimensions

The third system is the full three-dimensional hydrogen exchange reaction H+H_2 → H_2+H and its isotope variants, D+D_2 → D_2+D, and H+DH → HD+H, on the more accurate BKMP2 potential surface.[68,69,73]

1. Quantum instanton calculation

Again, due to the translational symmetry, we could subtract the center-of-mass-motion and make this system effectively six-dimensional, but instead (in the QI calculation) we use simple Cartesian coordinates and treat the reaction as a system with nine degrees of freedom. From this point of view, six translational, two rotational, and one vibrational degree of freedom of the reactants turn into three translational, two rotational, and four vibrational degrees of freedom of the collinear transition state (a symmetric and an asymmetric stretch, and two degenerate bending motions). The high temperature limit (5.8) becomes

$$r_{\mathrm{high}\ T} = \frac{s^{\ddagger}(1)}{s^{\ddagger}(0)} \left| \frac{\omega^{\ddagger}_{\mathrm{asym}}(0)}{\omega^{\ddagger}_{\mathrm{asym}}(1)} \right| \left\{ 1 + \frac{1}{24} \left(\frac{\hbar}{k_B T} \right)^2 \left[\Omega^2_{\mathrm{3D}}(0) - \Omega^2_{\mathrm{3D}}(1) \right] \right\}, \tag{7.11}$$

$$\Omega^2_{\mathrm{3D}}(\lambda) = \Omega^2_{\mathrm{coll}}(\lambda) - 2k_{\mathrm{bend}}/\mu_{\mathrm{AC,B}}(\lambda)\,.$$

where $k^{\ddagger}_{\mathrm{bend}}$ is the force constant of the bending motion. For the BKMP2 potential[68,69] the values of the force constants are $k_r = 0.3698$ a.u., $k^{\ddagger}_{\mathrm{asym}} = -0.0579$ a.u., $k^{\ddagger}_{\mathrm{sym}} = 0.0805$ a.u., and $k^{\ddagger}_{\mathrm{bend}} = 0.0209$ a.u. [Again, using the mass-scaled normal mode coordinates with a

common mass $\mu_{\rm AC,B}$ would give $k^{\ddagger}_{\rm sym} \to k^{\ddagger}_{\rm sym} \times (4/3) = 0.1073$ a.u.] Because of the symmetry of the potential, to find the normal modes we do not have to diagonalize a 4×4 matrix. The bending modes decouple, so in general we have to diagonalize only a 2×2 matrix coupling the symmetric and asymmetric stretch. However, because all three reactions considered here are symmetric, as in the collinear case, even this smaller matrix is already diagonal, and $|\omega^{\ddagger}_{\rm asym}(0)/\omega^{\ddagger}_{\rm asym}(1)| = [\mu_{\rm AC,B}(1)/\mu_{\rm AC,B}(0)]^{1/2}$. The classical limit (5.7) then gives $r_{\rm class}$(H+H_2 / D+D_2) $= \sqrt{2} \approx 1.414$ and $r_{\rm class}$(H+H_2 / H+DH) $= 2\sqrt{3/2} \approx 2.449$.

2. Exact cumulative reaction probabilities and rate constants

The exact quantum-mechanical kinetic isotope ratios were computed using the method described in Sec. VI. The exact total cumulative reaction probabilities, $N(E) = \sum_J (2J + 1) N^J(E)$, for the H+$H_2$, D+$D_2$ and H+HD→HD+H, →H_2+D are shown in Fig. 3 as a function of the total energy. The resulting $N(E)$ are fairly smooth and the higher values correspond to the D+D_2 reaction for all energies. Those for the two reaction arrangement channels of the H+HD reaction are fairly similar (for the D+H_2 channel no nuclear spin restriction has been enforced). As expected, the lowest values of the total CRP correspond to the H+H_2 reaction, whose threshold is similar to those of the H+HD reactions.

The values of the rate constants, $k(T)$ for all the isotopic variants here studied are shown in Table VII. The Arrhenius plot of these $k(T)$ is shown in Fig. 4. The existing experimental values for the H+H_2,[75] D+D_2,[76] and H+HD→D+H_2[76] are also shown in this figure. The agreement with these values is quite good, especially considering that these probably were the first measurements of $k(T)$ for these reactions.

3. Kinetic isotope effects

The kinetic isotope effect k(H+H_2) / k(D+D_2) for temperatures from 200 K to 2400 K is displayed in Fig. 5(a) and Table VIII. Besides the QM, QI, SQI, and high T TST values, this figure and table also display comparable results of the canonical variational TST with semiclassical tunneling (CVT-SCT) from Ref. 15 (that calculation was done for a slightly different—DMBE—potential[77,78]). For temperatures from 200 K to 600 K, the agreement between the QI and QM results is excellent: the error is less than 6% in this

temperature range. For high temperatures, the QI, SQI, and CVT-SCT results approach the classical behavior predicted by Eq. (7.11), as expected, because quantum effects become small. However, the QM results for 1000 K and 1500 K deviate significantly (15% and 19%, respectively). While in the collinear case we understood the increased error of the QI approximation at high temperatures to be due to recrossing effects, in three spatial dimensions these effects should be much smaller.[74] Moreover, as in the collinear case, the errors due to recrossing should partially cancel in the kinetic isotope ratio. Originally, we thought of another possible explanation: while QI calculations are easier to converge at high T (because fewer path variables are needed in the path integral), QM calculations become more difficult since more excited states must be included in Eq. (6.1). We therefore made sure that the QM calculations of Sec. VI were well converged even for high temperatures (1000 K and 1500 K). The reason for this somewhat higher error of the QI approximation for the KIE at high T still needs to be better understood. Comparing the QI and the CVT-SCT approximations shows that the QI method performs significantly better in the whole temperature range.

The corresponding results for the kinetic isotope effect $k(\mathrm{H+H_2})$ / $k(\mathrm{H+DH})$ are displayed in Fig. 5(b) and Table IX. One immediately observes that at high temperatures, the KIE $k(\mathrm{H+H_2})$ / $k(\mathrm{H+DH})$ is larger than the KIE $k(\mathrm{H+H_2}\ )$ / $k(\mathrm{D+D_2})$, whereas in the collinear case the situation was opposite. The reason is simple: in three spatial dimensions there are two identical product channels for the $\mathrm{H+H_2}$ or $\mathrm{D+D_2}$, but only one product channel (HD+H) of the reaction H+DH contributes to the KIE $k(\mathrm{H+H_2})$ / $k(\mathrm{H+DH})$. In the temperature range from 250 K to 600 K, the QI and QM results are in excellent agreement (the error is within 8%). At 200 K, a slightly higher error (11%) is due the use of a single dividing surface. At high temperatures (1000 K and 1500 K), the error is higher (16% and 19%) and, as for the previous KIE, still needs to be better understood. In any case, even 10-20% errors are excellent results, better than most approximate methods for computing KIEs. The errors for very low temperatures (below 250 K) could be avoided by using two separate dividing surfaces and evolving them according to the general prescription in Appendix B. Temperatures of interest in most chemical and biochemical applications are safely in the range 250 K and 600 K where the QI approximation, even with a single dividing surface, gives excellent results: less than 8% errors for both reactions. As in the previous case, the QI significantly outperforms the CVT-SCT approximation in the whole temperature range.

VIII. CONCLUSION

We have described a general and accurate method for computing the kinetic isotope effects (KIEs) and compared it on several test problems with the quantum-mechanical calculations and conventional and variational transition state theory (TST). Our method is based on the thermodynamic integration with respect to the masses of the isotopes, the quantum instanton (QI) approximation for the rate constant, and on the path integral Monte Carlo (PIMC) evaluation of the matrix elements of the Boltzmann operator. The several examples presented here demonstrate that the QI method is more accurate than simpler TST approaches based on a single reaction path. For similar reasons, the QI approximation is also superior to the older SC instanton approximation.

We have theoretically described two versions of the method: with a single or two separate dividing surfaces. Using a single dividing surface is more efficient and already gives less than $\sim$10% error for the KIEs in the temperature range 250 K to 600 K for all seven test cases considered. The slightly higher error at lower temperatures could be reduced by using two separate dividing surfaces. At high temperatures ($\geq$ 1000 K), a slightly higher error is partially due to classical recrossing effects, which are not accounted for by the QI in its present form. However, recrossing effects become less important as the number of degrees of freedom increases. In particular, it should be negligible for polyatomic systems even at quite high temperatures.

Finally, an important feature of the method is its computational efficiency. One reason is the Metropolis PIMC implementation that scales favorably with the number of degrees of freedom. Another reason is that we evaluate the KIEs directly, using a thermodynamic integration with respect to the mass of the isotope, instead of finding the absolute rate constants for the two isotopologues first and then computing their ratio. Thus we avoid the cumbersome umbrella sampling that is required in computation of the absolute rate constants.

There are several avenues available to further enhance the accuracy and efficiency of the present methodology, such as: a) the inclusion of higher order derivatives of the flux-flux correlation function at the origin (this approach should lead to an *exact* rate in the limit),[41,79,80] b) capturing the classical recrossing effects by SC methods,[81–86] c) using a smaller number of path variables for heavier atoms or less important degrees of freedom

(which could increase the efficiency without effecting the accuracy),[42] and d) a general search algorithm for the optimal dividing surfaces. The goal of this overall approach, of course, is to implement the methodology to realistic models of molecular systems with many degrees of freedom.

Acknowledgments

This work was supported by the Director, Office of Science, Office of Basic Energy Sciences, Chemical Sciences, Geosciences, and Biosciences Division, U.S. Department of Energy under Contract No. DE-AC03-76SF00098, by the National Science Foundation Grant No. CHE-0345280, and by DGES of Spain (Project BQU2002-04627-C02-02). JV would like to thank Yimin Li and the rest of Bill Miller's group for many useful discussions. JFC acknowledges support through the program "Ramon y Cajal" from the Ministry of Education and Culture of Spain.

APPENDIX A: ESTIMATORS FOR C_{ff}/C_{dd} AND ΔH

For completeness we write out explicitly the estimators for $C_{ff}(0)_\lambda / C_{dd}(0)_\lambda$ and ΔH_λ for the case when a Gaussian approximation of the delta constraint (4.12) and the corresponding constrained density (4.14) are used. It is a generalization of estimators from Ref. 37,

$$\frac{C_{ff}(0)_\lambda}{C_{dd}(0)_\lambda} \simeq \left\langle f_v\left(\left\{\mathbf{r}^{(s)}\right\}\right)\right\rangle_{\rho^\ddagger}, \tag{A1}$$

$$\Delta H_\lambda^2 \simeq \frac{1}{2}\left\langle F\left(\left\{\mathbf{r}^{(s)}\right\}\right)^2 + G\left(\left\{\mathbf{r}^{(s)}\right\}\right)\right\rangle_{\rho^\ddagger}, \tag{A2}$$

with velocity factor

$$f_v\left(\left\{\mathbf{r}^{(s)}\right\}\right) = \left(\frac{iP}{\hbar\beta}\right)^2 \frac{\nabla\zeta\left(\bar{\mathbf{r}}^{(1)}\right)\cdot\left(\mathbf{r}^{(1)}-\mathbf{r}^{(P)}\right)}{\left\|\nabla\zeta\left(\bar{\mathbf{r}}^{(1)}\right)\right\|_-} \frac{\nabla\zeta\left(\bar{\mathbf{r}}^{(P/2+1)}\right)\cdot\left(\mathbf{r}^{(P/2+1)}-\mathbf{r}^{(P/2)}\right)}{\left\|\nabla\zeta\left(\bar{\mathbf{r}}^{(P/2+1)}\right)\right\|_-}, \tag{A3}$$

and

$$F\left(\left\{\mathbf{r}^{(s)}\right\}\right) = -\frac{P^2}{2\hbar^2\beta^2}\sum_{s=1}^{P} a_s \left\|\mathbf{r}^{(s)}-\mathbf{r}^{(s-1)}\right\|_+^2 + \sum_{s=1}^{P} b_s V\left(\mathbf{r}^{(s)}\right), \tag{A4}$$

$$G\left(\left\{\mathbf{r}^{(s)}\right\}\right) = \frac{NdP^2}{2\beta^2}\sum_{s=1}^{P} a_s^2 - \frac{P^3}{\hbar^2\beta^3}\sum_{s=1}^{P} a_s^2 \left\|\mathbf{r}^{(s)}-\mathbf{r}^{(s-1)}\right\|_+^2. \tag{A5}$$

Here $\|\mathbf{r}\|_+$ denotes the norm of a contravariant vector $\mathbf{r}$,

$$\|\mathbf{r}\|_+ = \sqrt{\sum_{i=1}^{N} m_i \mathbf{r}_i^2} \tag{A6}$$

[the "+" sign subscript on the left-hand side denotes that the positive first power of m_i must be used in the norm of a contravariant vector, compare with Eq. (2.10)]. The dot $(\cdot)$ in Eq. (A3) denotes the dual product between a covariant vector $\mathbf{x}$ and a contravariant vector $\mathbf{y}$,

$$\mathbf{x} \cdot \mathbf{y} = \sum_{i=1}^{N} \mathbf{x}_i \cdot \mathbf{y}_i. \tag{A7}$$

[The dot $(\cdot)$ on the right hand side denotes the usual scalar product in three-dimensional space.]

APPENDIX B: EVOLUTION OF THE DIVIDING SURFACES

When the symmetry of the reaction is broken by the isotope change, the location of optimal dividing surfaces will in general depend on λ. For simplicity, we assume that the dependence of ξ on position $\mathbf{r}$ and parameter λ can be separated, so

$$\xi_\gamma (\mathbf{r}, \lambda) = \zeta (\mathbf{r}) - \eta_\gamma (\lambda), \tag{B1}$$

[I. e., in Eq. (4.9), we only have two parameters η_a, η_b controlling the position of the dividing surfaces along a single "reaction" coordinate ζ.] In order to find out how the dividing surfaces evolve with changing λ, we first recall that C_{dd} has both explicit and implicit dependence on λ, $C_{dd} \equiv C_{dd} [\lambda, \eta_a (\lambda), \eta_b (\lambda)]$, and then differentiate Eq. (2.11) with respect to λ,

$$\frac{d}{d\lambda} \frac{\partial C_{dd}}{\partial \eta_\alpha} = \frac{\partial^2 C_{dd}}{\partial \lambda \partial \eta_\alpha} + \sum_{\beta=a,b} \frac{\partial^2 C_{dd}}{\partial \eta_\alpha \partial \eta_\beta} \frac{d\eta_\beta}{d\lambda} = 0. \tag{B2}$$

This equation can be easily solved to obtain $d\eta_\alpha / d\lambda$. The solution is conveniently expressed in terms of a 2×2 matrix A and a 2-vector B,

$$A_{\alpha\beta} = \frac{\partial^2 C_{dd} / \partial \eta_\alpha \partial \eta_b}{C_{dd}}, \tag{B3}$$

$$B_\alpha = \frac{\partial^2 C_{dd} / \partial \lambda \partial \eta_\alpha}{C_{dd}}, \tag{B4}$$

as

$$\frac{d\eta_\alpha}{d\lambda} = -\sum_{\beta=a,b} A^{-1}_{\alpha\beta} B_\beta. \tag{B5}$$

[We have divided Eq. (B2) by C_{dd} in order that A and B be normalized and ready for PIMC evaluation.] Knowing the position of the dividing surface for $\lambda = 0$, we can simultaneously integrate Eqs. (4.13) and (B5) to obtain the ratio $C_{dd}(\lambda)/C_{dd}(0)$ and the position of dividing surfaces for each λ. PIMC estimators for A, B, and $\partial \log C_{dd}/\partial\lambda$ can be compactly written as,

$$A_{\alpha\beta} \simeq \langle f_{\alpha\beta} + f_\alpha f_\beta \rangle_{\rho^\ddagger}, \tag{B6}$$

$$B_\alpha \simeq \langle f_{\lambda\alpha} + f_\lambda f_\alpha \rangle_{\rho^\ddagger}, \tag{B7}$$

$$\frac{\partial \log C_{dd}}{\partial\lambda} \simeq \langle f_\lambda \rangle_{\rho^\ddagger}, \tag{B8}$$

where $\rho^\ddagger$ is the constrained density (4.14) and

$$f_\lambda = \sum_{i=1}^{N} \frac{dm_i}{d\lambda} \left[\frac{dP}{2m_i} - \beta \frac{\partial \Phi}{\partial m_i} - \frac{2P}{\hbar^2\beta} \sum_{\gamma=a,b} \frac{\xi_\gamma(\mathbf{r},\lambda)^2 |\nabla_i \zeta|^2}{m_i^2 \|\nabla\zeta\|_-^4} \right], \tag{B9}$$

$$f_\alpha = \frac{4P}{\hbar^2\beta} \frac{\xi_\alpha(\mathbf{r},\lambda)}{\|\nabla\zeta\|_-^2}, \tag{B10}$$

$$f_{\lambda\alpha} = \frac{4P}{\hbar^2\beta} \frac{\xi_\alpha(\mathbf{r},\lambda)}{\|\nabla\zeta\|_-^4} \sum_{i=1}^{N} \frac{dm_i/d\lambda}{m_i^2} |\nabla_i\zeta|^2, \tag{B11}$$

$$f_{\alpha\beta} = -\delta_{\alpha\beta} \frac{4P}{\hbar^2\beta} \frac{1}{\|\nabla\zeta\|_-^2}. \tag{B12}$$

* Electronic address: vanicek@post.harvard.edu

[1] L. C. S. Melander, *Isotope effects on reaction rates* (Ronald Press Co., New York, 1960).

[2] C. J. Collins and E. N. S. Bowman, *Isotope effects in chemical reactions* (Van Nostrand Reinhold, New York, 1971).

[3] E. J. A. Kaye, *Isotope effects in gas-phase chemistry* (American Chemical Society, Washington, DC, 1992).

[4] A. Kohen, R. Cannio, S. Bartolucci, and J. P. Klinman, Nature **399**, 496 (1999).

[5] A. Kohen and J. P. Klinman, J. Am. Chem. Soc. **122**, 10738 (2000).

[6] M. J. Knapp, K. Rickert, and J. P. Klinman, J. Am. Chem. Soc. **124**, 3865 (2002).

[7] M. J. Knapp and J. P. Klinman, Eur. J. Biochem. **269**, 3113 (2002).

[8] J. Basran, M. J. Sutcliffe, and N. S. Scrutton, Biochemistry **38**, 3218 (1999).

[9] J. Basran, S. Patel, M. J. Sutcliffe, and N. S. Scrutton, J. Biol. Chem. **276**, 6234 (2001).

[10] M. J. Sutcliffe and N. S. Scrutton, Eur. J. Biochem. **269**, 3096 (2002).

[11] J. Bigeleisen and M. Wolfsberg, Adv. Chem. Phys. **1**, 15 (1958).

[12] E. P. Wigner, Z. Physik. Chem. **B19**, 903 (1932).

[13] R. A. Marcus and M. E. Coltrin, J. Chem. Phys. **67**, 2609 (1977).

[14] W. H. Miller, J. Phys. Chem. **87**, 3811 (1983).

[15] P. L. Fast, J. C. Corchado, and D. G. Truhlar, J. Chem. Phys. **109**, 6237 (1998).

[16] W. H. Miller, J. Chem. Phys. **62**, 1899 (1975).

[17] S. Coleman, Phys. Rev. D **15**, 2929 (1977).

[18] W. H. Miller, Acc. Chem. Res. **26**, 174 (1993).

[19] W. H. Miller, Faraday Discuss. **110**, 1 (1998).

[20] K. Yamashita and W. H. Miller, J. Chem. Phys. **82**, 5475 (1985).

[21] J. W. Tromp and W. H. Miller, J. Phys. Chem. **90**, 3482 (1986).

[22] G. A. Voth, D. Chandler, and W. H. Miller, J. Chem. Phys. **91**, 7749 (1989).

[23] G. A. Voth, D. Chandler, and W. H. Miller, J. Phys. Chem. **93**, 7009 (1989).

[24] A. Gonzalezlafont, S. N. Rai, G. C. Hancock, T. Joseph, and D. G. Truhlar, Chem. Phys. Lett. **75**, 143 (1993).

[25] N. F. Hansen and H. C. Andersen, J. Chem. Phys. **101**, 6032 (1994).

[26] N. F. Hansen and H. C. Andersen, J. Phys. Chem. **100**, 1137 (1996).

[27] E. Pollak and J. L. Liao, J. Chem. Phys. **108**, 2733 (1998).

[28] J. Shao, J. L. Liao, and E. Pollak, J. Chem. Phys. **108**, 9711 (1998).

[29] W. H. Miller, J. Phys. Chem. **103**, 9384 (1999).

[30] S. Jang and G. A. Voth, J. Chem. Phys. **112**, 8747 (2000).

[31] E. Sim, G. Krilov, E. Sim, and B. J. Berne, J. Phys. Chem. A **105**, 2824 (2001).

[32] G. Krilov, E. Sim, and B. J. Berne, J. Chem. Phys. **114**, 1075 (2001).

[33] S.-Y. Kim and S. Hammes-Schiffer, J. Chem. Phys. **119**, 4389 (2003).

[34] M. H. M. Olsson, P. E. M. Siegbahn, and A. Warshel, J. Am. Chem. Soc. **126**, 2820 (2003).

[35] W. H. Miller, Y. Zhao, M. Ceotto, and S. Yang, J. Chem. Phys. **119**, 1329 (2003).

[36] S. Chapman, B. C. Garrett, and W. H. Miller, J. Chem. Phys. **63**, 2710 (1975).

[37] T. Yamamoto and W. H. Miller, J. Chem. Phys. **120**, 3086 (2004).

[38] Y. Zhao, T. Yamamoto, and W. H. Miller, J. Chem. Phys. **120**, 3100 (2004).

[39] M. Ceotto and W. H. Miller, J. Chem. Phys. **120**, 6356 (2004).

[40] C. Venkataraman and W. H. Miller, J. Phys. Chem. A **108**, 3035 (2004).

[41] W. H. Miller, M. Ceotto, and S. Yang, J. Chem. Phys. **122**, 044109 (2005).

[42] Y. Li and W. H. Miller, Mol. Phys. **103**, 203 (2004).

[43] R. P. Feynman and A. R. Hibbs, *Quantum mechanics and path integrals* (McGraw-Hill, New York, 1965).

[44] R. P. Feynman, *Statistical mechanics* (Benjamin, New York, 1972).

[45] D. M. Ceperley, Rev. Mod. Phys. **67**, 279 (1995).

[46] D. Frenkel and B. Smit, *Understanding molecular simulation* (Academic Press, San Diego, 1996).

[47] D. Chandler, *Introduction to modern statistical mechanics* (Oxford University Press, New York, 1987).

[48] T. Yamamoto and W. H. Miller, J. Chem. Phys. **122**, 044106 (2005).

[49] M. Ceotto and W. H. Miller, not published.

[50] W. H. Miller, S. D. Schwartz, and J. W. Tromp, J. Chem. Phys. **79**, 4889 (1983).

[51] O. Redlich, Z. Physik. Chem. **B28**, 371 (1935).

[52] E. Teller, quoted by Angus et al., J. Chem. Soc. **62**, 971 (1936).

[53] D. G. Truhlar and A. Kuppermann, J. Chem. Phys. **56**, 2232 (1972).

[54] D. G. Truhlar and J. C. Gray, not published.

[55] D. G. Truhlar, A. Kuppermann, and J. T. Adams, J. Chem. Phys. **59**, 395 (1973).

[56] J. C. Gray, B. C. Garret, and D. G. Truhlar, not published.

[57] W. H. Miller, J. Chem. Phys. **62**, 1899 (1975).

[58] S. L. Mielke, G. C. Lynch, D. G. Truhlar, and D. W. Schwenke, Chem. Phys. Lett. **213**, 11 (1993).

[59] S. L. Mielke, G. C. Lynch, D. G. Truhlar, and D. W. Schwenke, J. Phys. C **98**, 8000 (1994).

[60] D. Skouteris, J. F. Castillo, and D. E. Manolopoulos, Comp. Phys. Comm. **113**, 128 (2000).

[61] J. F. Castillo, D. E. Manolopoulos, K. Stark, and H.-J. Werner, J. Chem. Phys. **104**, 6531 (1996).

[62] J. F. Castillo, B. Hartke, H.-J. Werner, F. J. Aoiz, L. Bañares, and B. Martínez-Haya, J. Chem. Phys. **109**, 7224 (1998).

[63] F. J. Aoiz, L. Bañares, and J. F. Castillo, J. Chem. Phys. **111**, 4013 (1999).

[64] J. F. Castillo and D. E. Manolopoulos, Faraday Discuss. Chem. Soc. **110**, 119 (1998).

[65] M. P. de Miranda, D. C. Clary, J. F. Castillo, and D. E. Manolopoulos, J. Chem. Phys. **108**, 3142 (1988).

[66] E. Wrede, L. Schnieder, K. H. Welge, F. J. Aoiz, L. Bañares, J. F. Castillo, B. Martínez-Haya, and V. J. Herrero, J. Chem. Phys. **110**, 9971 (1999).

[67] T. Xie, D. Y. Wang, J. M. Bowman, and D. E. Manolopoulos, J. Chem. Phys. **116**, 7461 (2002).

[68] A. I. Boothroyd, W. J. Keogh, P. G. Martin, and M. R. Peterson, J. Chem. Phys. **104**, 7139 (1996).

[69] A. I. Boothroyd, W. J. Keogh, P. G. Martin, and M. R. Peterson, J. Chem. Phys. **95**, 4343 (1991).

[70] M. Sprik, M. L. Klein, and D. Chandler, Phys. Rev. B **31**, 4234 (1985).

[71] M. Sprik, M. L. Klein, and D. Chandler, Phys. Rev. B **32**, 545 (1985).

[72] M. E. Tuckerman, B. J. Berne, G. J. Martyna, and M. L. Klein, J. Chem. Phys. **99**, 2796 (1993).

[73] R. J. Duchovic, Y. L. Volobuev, G. C. Lynch, A. W. Jasper, D. G. Truhlar, T. C. Allison, A. F. Wagner, B. C. Garrett, J. Espinosa-García, and J. C. Corchado, POTLIB-online, `http://comp.chem.umn.edu/potlib`.

[74] W. H. Miller, J. Am. Chem. Soc. **97**, 892 (1975).

[75] K. Geib and P. Harteck, Z. Physik. Chem. Bodenstein Festband p. 849 (1931).

[76] A. Farkas and L. Farkas, Proc. Roy. Soc. A **152**, 124 (1935).

[77] A. J. C. Varandas, F. B. Brown, C. A. Mead, D. G. Truhlar, and N. C. Blais, J. Chem. Phys. **86**, 6258 (1987).

[78] B. C. Garrett, D. G. Truhlar, A. J. C. Varandas, and N. C. Blais, Int. J. Chem. Kinet. **18**, 1065 (1986).

[79] C. Predescu and J. D. Doll, J. Chem. Phys. **117**, 7448 (2002).

[80] C. Predescu, J. Chem. Phys. **70**, 066705 (2004).

[81] W. H. Miller, J. Phys. Chem. **105**, 2942 (2001).

[82] W. H. Miller, J. Phys. Chem. **105**, 2942 (2001).

[83] J. Vaníček and E. J. Heller, Phys. Rev. E **67**, 016211 (2003).

[84] J. Vaníček and E. J. Heller, Phys. Rev. E **68**, 056208 (2003).

[85] J. Vaníček, Ph.D. thesis, Harvard University (2003), `http://physics.harvard.edu/Thesespdfs/vanicek.pdf`

[86] J. Vaníček, Phys. Rev. E **70**, 055201(R) (2004).

[87] This expression is for a bimolecular reaction. In the limit $V \to \infty$, V^{-2} cancels the V^2 divergence from the integration over the center-of-mass coordinate and the relative coordinate of the two molecules. For a unimolecular reaction, the factor is V^{-1} and is canceled by integration over the center-of-mass coordinate.

[88] Factor V^{-1} is canceled by the integral over the center of mass coordinate. Expression (4.7) is valid for both unimolecular and bimolecular reactions.

[89] To make sure that there was no "leakage" into the other product channel (AC+B), we also used $\zeta = \min(\zeta_1, \zeta_2)$ where $\zeta_1 = r_{\mathrm{BC}} - r_{\mathrm{AB}}$ and $\zeta_2 = r_{\mathrm{AC}} - r_{\mathrm{AB}}$.

[90] While $m_0 = 1060$ a.u. is not the correct reduced mass corresponding to the H + H_2 →H_2 + H reaction, we use this numerical value since it has been used extensively in literature.

TABLES

TABLE I: Size of the basis set employed in the exact QM scattering calculations for the H+H_2 reaction and isotopic variants on the BKMP2 PES.

J	Reaction	Diatomic parity	Triatomic Parity	Number of channels
0	H+p–H_2	$(-1)^j$=1	$(-1)^p$=$(-1)^J$	108
1	H+p–H_2	$(-1)^j$=1	$(-1)^p$=$(-1)^J$	204
1	H+p–H_2	$(-1)^j$=1	$(-1)^p$=$(-1)^{J+1}$	96
≥7, even	H+p–H_2	$(-1)^j$=1	$(-1)^p$=$(-1)^J$	614
≥7, even	H+p–H_2	$(-1)^j$=1	$(-1)^p$=$(-1)^{J+1}$	506
≥7, odd	H+p–H_2	$(-1)^j$=1	$(-1)^p$=$(-1)^J$	614
≥7, odd	H+p–H_2	$(-1)^j$=1	$(-1)^p$=$(-1)^{J+1}$	506
0	D+p–D_2	$(-1)^j$=1	$(-1)^p$=$(-1)^J$	171
1	D+o–D_2	$(-1)^j$=1	$(-1)^p$=$(-1)^J$	346
1	D+o–D_2	$(-1)^j$=1	$(-1)^p$=$(-1)^{J+1}$	165
≥7, even	D+p–D_2	$(-1)^j$=1	$(-1)^p$=$(-1)^J$	1098
≥7, even	D+p–D_2	$(-1)^j$=1	$(-1)^p$=$(-1)^{J+1}$	917
≥7, odd	D+p–D_2	$(-1)^j$=1	$(-1)^p$=$(-1)^J$	1098
≥7, odd	D+p–D_2	$(-1)^j$=1	$(-1)^p$=$(-1)^{J+1}$	917
0	H+ –HD	$(-1)^j$=0	$(-1)^p$=$(-1)^J$	251
1	H+ –HD	$(-1)^j$=0	$(-1)^p$=$(-1)^J$	484
1	H+ –HD	$(-1)^j$=0	$(-1)^p$=$(-1)^{J+1}$	233
≥7, even	H+ –HD	$(-1)^j$=0	$(-1)^p$=$(-1)^J$	1514
≥7, even	H+ –HD	$(-1)^j$=0	$(-1)^p$=$(-1)^{J+1}$	1263
≥7, odd	H+ –HD	$(-1)^j$=0	$(-1)^p$=$(-1)^J$	1514
≥7, odd	H+ –HD	$(-1)^j$=0	$(-1)^p$=$(-1)^{J+1}$	1263

TABLE II: Kinetic isotope effect $r = k_{\rm H}/k_{\rm D}$ for the Eckart barrier: $r_{\rm QI}$ is the quantum instanton result obtained from Eq. (3.3), $r_{\rm SQI}$ the "simplest" quantum instanton from Eq. (7.2), $r_{\rm QI}^{\rm mod}$ the "modified" quantum instanton from Eq. (3.3) with ΔH replaced by Eq. (7.3), $r_{\rm TST}^{{\rm high}T}$ the high T expansion of the TST from Eq. (7.5), and $r_{\rm QM}$ is the ratio of rate constants obtained from Eqs. (2.1) and (7.6).

T(K)	$r_{\rm QI}$	% error[a]	$r_{\rm SQI}$	% error[b]	$r_{\rm QI}^{\rm mod}$	% error[c]	$r_{\rm TST}^{{\rm high}T}$	% error [d]	$r_{\rm QM}$
100	1509	-15	1134	-36	1482	-16	17.43	-99	1767
150	266.3	-10	154.3	-48	263.0	-11	8.53	-97	296.8
200	42.75	-20	25.96	-52	42.79	-20	5.42	-90	53.60
300	6.20	-5	4.71	-28	6.34	-3	3.19	-51	6.535
400	3.18	2	2.71	-13	3.27	5	2.41	-23	3.125
600	2.00	1	1.87	-6	2.05	3	1.86	-6	1.987
1000	1.59	-1	1.56	-3	1.61	0	1.57	-2	1.609
1500	1.49	-1	1.48	-2	1.50	0	1.49	-1	1.506
2400	1.43	-2	1.44	-1	1.43	-2	1.44	-1	1.455
∞							1.414	0	1.414

[a] $(k_{\rm QI} - k_{\rm QM})/k_{\rm QM} \times 100$
[b] $(k_{\rm SQI} - k_{\rm QM})/k_{\rm QM} \times 100$
[c] $(k_{\rm QI}^{\rm mod} - k_{\rm QM})/k_{\rm QM} \times 100$
[d] $(k_{\rm TST}^{{\rm high}T} - k_{\rm QM})/k_{\rm QM} \times 100$

TABLE III: Kinetic isotope effect $r = k_{H+H_2}/k_{D+D_2}$ for the collinear reaction using the TK potential.[53] Here $r_{TST}^{high T}$ was obtained from Eq. (7.8), r_{QM} from Refs. 53,55. Meaning of remaining quantities is the same as in Tab. II.

T(K)	r_{QI}	% error	r_{SQI}	% error	r_{QI}^{mod}	% error	$r_{TST}^{high T}$	% error	r_{QM}
200	59.57	-23	42.21	-45	60.87	-21	28.85	-63	77.24
300	10.87	3	10.28	-3	11.18	5	13.61	28	10.60
400	6.21	7	5.93	2	6.29	7	8.27	42	5.81
600	3.75	7	3.54	1	3.75	7	4.46	27	3.51
1000	2.37	-1	2.28	-5	2.37	-1	2.51	5	2.39
1500	1.81	-5	1.82	-5	1.82	-5	1.90	0	1.91
∞							1.41		

TABLE IV: Kinetic isotope effect $r = k_{\mathrm{H+H_2}}/k_{\mathrm{H+DH}}$ for the collinear reaction using the TK potential.[53] Meaning of various quantities is the same as in Tab. III.

T(K)	r_{QI}	r_{SQI}	$r_{\mathrm{QI}}^{\mathrm{mod}}$	$r_{\mathrm{TST}}^{\mathrm{high}T}$
200	14.06	11.50	14.04	16.28
300	5.22	4.89	5.24	7.92
400	3.45	3.32	3.45	4.99
600	2.36	2.27	2.35	2.90
1000	1.69	1.67	1.69	1.83
1500	1.43	1.44	1.43	1.49
∞				1.22

TABLE V: Kinetic isotope effect $r = k_{H+H_2}/k_{D+H_2}$ for the collinear reaction using the TK potential.[53] Meaning of various quantities is the same as in Tab. III.

T(K)	r_{QI}	% error	r_{SQI}	% error	r_{QI}^{mod}	% error	$r_{TST}^{high T}$	% error	r_{QM}
200	1.002	4	0.396	-59	0.999	3	-0.738	-176	0.967
300	0.793	-2	0.600	-26	0.786	-3	0.258	-68	0.810
400	0.826	-5	0.722	-17	0.822	-6	0.606	-30	0.870
600	0.882	-11	0.863	-13	0.882	-11	0.855	-13	0.988
1000	0.994	-8	0.970	-11	0.992	-8	0.983	-9	1.084
1500	1.010	-14	1.008	-14	1.010	-14	1.022	-13	1.175
∞							1.054		

TABLE VI: Kinetic isotope effect $r = k_{H+H_2}/k_{H+D_2}$ for the collinear reaction using the TK potential.[53] Meaning of various quantities is the same as in Tab. III.

T(K)	r_{QI}	% error	r_{SQI}	% error	r_{QI}^{mod}	% error	$r_{TST}^{high T}$	% error	r_{QM}
200	127.3	-22	41.63	-74	126.0	-23	29.78	-82	163
300	17.92	-3	12.52	-32	17.69	-4	13.98	-25	18.52
400	8.31	-3	6.92	-19	8.20	-4	8.44	-1	8.56
600	4.11	-4	3.76	-13	4.08	-5	4.49	4	4.30
1000	2.31	-8	2.25	-10	2.31	-8	2.47	-2	2.51
1500	1.77	-12	1.75	-13	1.77	-12	1.84	-8	2.00
∞							1.33		

TABLE VII: Exact QM thermal rate constants $k(T)$ for the $H+H_2$ reaction and isotopic variants as a function of temperature calculated on the BKMP2 PES. The rate constants were obtained from Eq. (6.1). They are in units $cm.s^{-3}$, the figure in parentheses denoting the power of 10.

T(K)	$H+H_2$	$D+D_2$	$H+HD \rightarrow H+HD$	$H+HD \rightarrow D+H_2$
200	2.01(-18)	8.92(-20)	1.14(-19)	2.02(-19)
250	3.67(-17)	3.53(-18)	3.46(-18)	5.71(-18)
300	3.24(-16)	4.65(-17)	4.04(-17)	6.34(-17)
350	1.71(-15)	3.11(-16)	2.53(-16)	3.83(-16)
400	6.30(-15)	1.33(-15)	1.05(-15)	1.54(-15)
450	1.79(-14)	4.23(-15)	3.25(-15)	4.65(-15)
500	4.21(-14)	1.08(-14)	8.17(-15)	1.15(-14)
600	1.57(-13)	4.59(-14)	3.37(-14)	4.57(-14)
800	8.87(-13)	3.05(-13)	2.15(-13)	2.77(-13)
1000	2.69(-12)	1.03(-12)	7.01(-13)	8.71(-13)
1200	5.89(-12)	2.42(-12)	1.61(-12)	1.95(-12)
1500	1.35(-11)	5.96(-12)	3.87(-12)	4.55(-12)

TABLE VIII: Kinetic isotope effect $r = k_{\mathrm{H+H_2}}/k_{\mathrm{D+D_2}}$ for the reaction in three spatial dimensions, using the BKMP2 potential[68,69] except for $r_{\mathrm{CVT/SCT}}$ which uses the DMBE potential.[77,78] Here $r_{\mathrm{TST}}^{\mathrm{high}T}$ is the high T expansion of TST from Eq. (7.11), $r_{\mathrm{CVT/SCT}}$ is the result of canonical variational TST with semiclassical tunneling corrections from Ref. 15 and r_{QM} is the quantum-mechanical result from Eq. (6.1). Meaning of remaining quantities is the same as in Tab. III.

T(K)	r_{QI}	% err.	r_{SQI}	% err.	$r_{\mathrm{QI}}^{\mathrm{mod}}$	% err.	$r_{\mathrm{TST}}^{\mathrm{high}T}$	% err.	$r_{\mathrm{CVT/SCT}}$	% err.[a]	r_{QM}
200	23.35	4	16.66	-26	23.77	6	25.53	13	13.67	-39	22.53
250	10.98	6	9.10	-13	11.28	8	16.85	62	7.56	-27	10.40
300	7.41	6	6.42	-8	7.58	9	12.13	74	5.48	-21	6.97
400	4.84	2	4.41	-7	4.92	4	7.44	57	3.87	-18	4.74
600	3.25	-5	3.04	-11	3.29	-4	4.09	20			3.42
1000	2.22	-15	2.15	-18	2.24	-14	2.38	-9	2.03	-22	2.61
1500	1.83	-19	1.78	-22	1.84	-19	1.84	-19			2.27
2400	1.56		1.56		1.57		1.58		1.57		
∞							1.41				

[a] $(k_{\mathrm{CVT/SCT}} - k_{\mathrm{QM}})/k_{\mathrm{QM}} \times 100$

TABLE IX: Kinetic isotope effect $r = k_{H+H_2}/k_{H+DH}$ using the BKMP2 potential[68,69] except for $r_{CVT/SCT}$ which uses the DMBE potential.[77,78] Meaning of various quantities is the same as in Tab. VIII.

T(K)	r_{QI}	% error	r_{SQI}	% error	r_{QI}^{mod}	% error	$r_{TST}^{high T}$	% error	$r_{CVT/SCT}$	% error	r_{QM}
200	15.77	-11	12.88	-27	15.79	-10	29.19	66	8.21	-53	17.63
250	10.23	-4	8.99	-15	10.29	-3	19.56	84	6.58	-38	10.61
300	7.88	-2	7.08	-12	7.91	-1	14.33	79	5.66	-29	8.02
400	5.84	-3	5.38	-10	5.86	-2	9.13	52	4.65	-22	6.00
600	4.27	-8	4.04	-13	4.29	-8	5.42	16			4.66
1000	3.21	-16	3.17	-17	3.23	-16	3.52	-8	3.06	-20	3.83
1500	2.81	-19	2.80	-19	2.82	-18	2.92	-15			3.45
2400	2.59		2.57		2.59		2.64		2.47		
∞							2.45				

FIGURE CAPTIONS

FIG. 1: Kinetic isotope effect $k_{\mathrm{H}}/k_{\mathrm{D}}$ for the Eckart barrier.

FIG. 2: Kinetic isotope effect for the collinear hydrogen exchange reaction: (a) $k(\mathrm{H}+\mathrm{H}_2)$ / $k(\mathrm{D}+\mathrm{D}_2)$, (b) $k(\mathrm{H}+\mathrm{H}_2)$ / $k(\mathrm{H}+\mathrm{DH} \rightarrow \mathrm{HD}+\mathrm{H})$, (c) $k(\mathrm{H}+\mathrm{H}_2)$ / $k(\mathrm{D}+\mathrm{H}_2)$, (d) $k(\mathrm{H}+\mathrm{H}_2)$ / $k(\mathrm{H}+\mathrm{D}_2)$.

Fig. 3: QM *total* cumulative reaction probabilities calculated using the BKMP2 PES for the H+*p*–H_2, D+*p*–D_2, and H+–HD reactions.

FIG. 4: QM rate constants calculated using the BKMP2 for the H+*p*–H_2, D+*p*–D_2, and H+–HD reactions.

FIG. 5: Kinetic isotope effect for the hydrogen exchange reaction in three spatial dimensions: (a) $k(\mathrm{H}+\mathrm{H}_2)$ / $k(\mathrm{D}+\mathrm{D}_2)$, (b) $k(\mathrm{H}+\mathrm{H}_2)$ / $k(\mathrm{H}+\mathrm{DH} \rightarrow \mathrm{HD}+\mathrm{H})$.

FIGURES

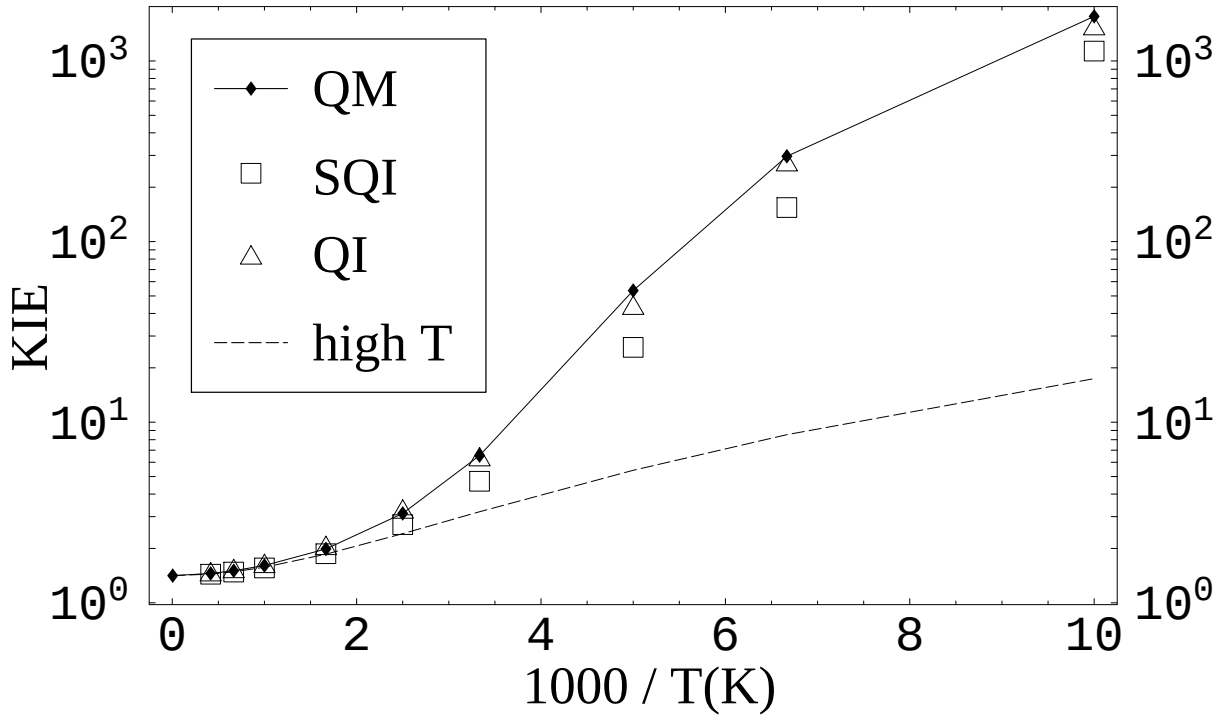

FIG. 1: J. Vanicek et al.

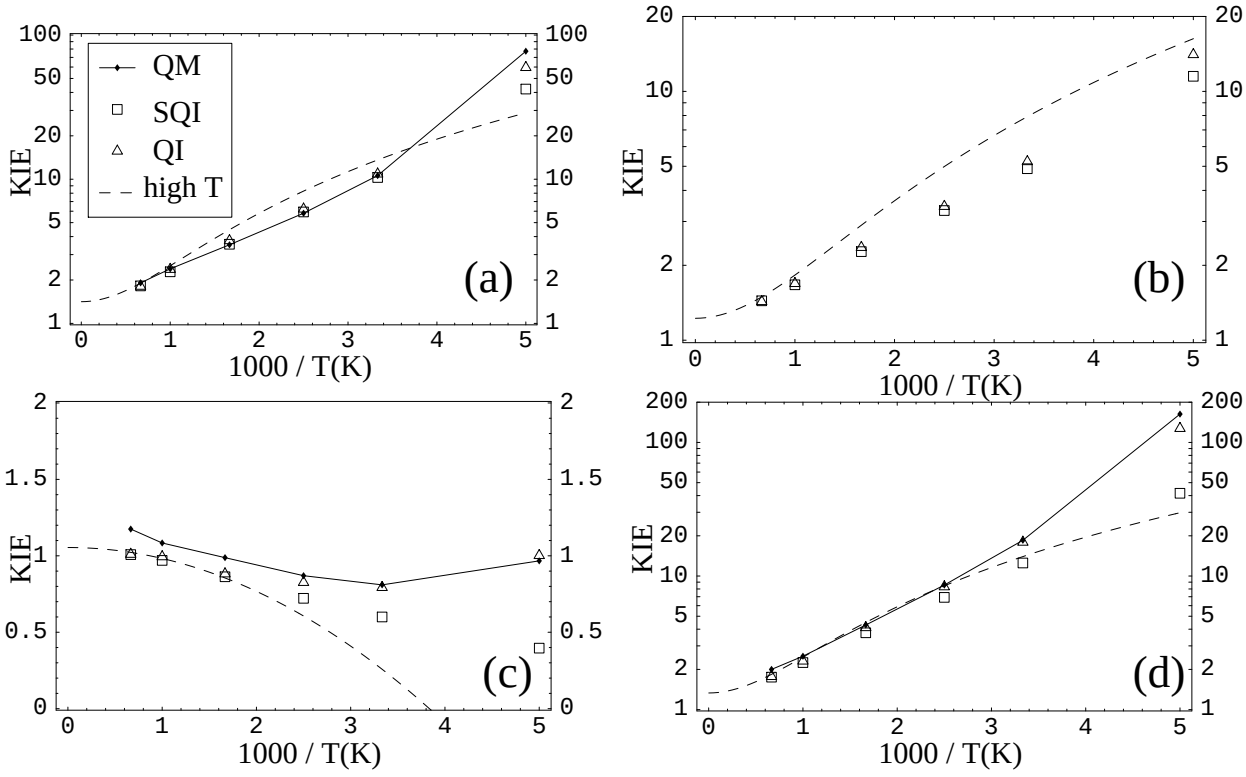

FIG. 2: J. Vanicek et al.

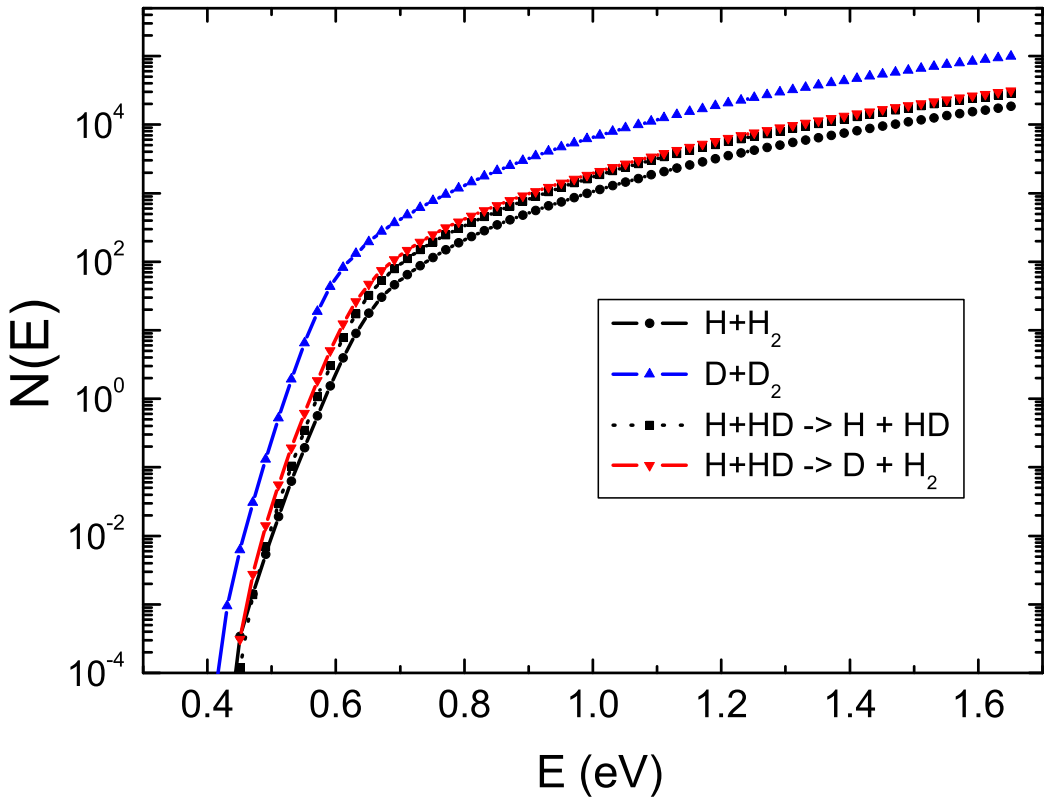

FIG. 3: J. Vanicek et al.

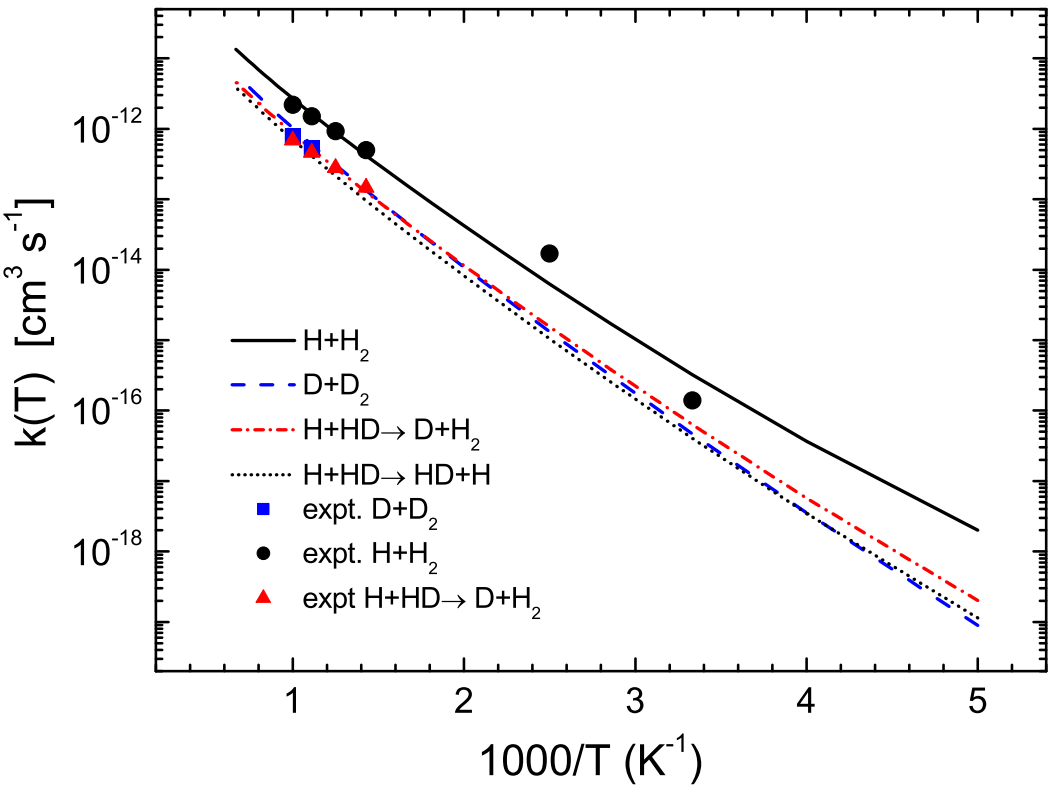

FIG. 4: J. Vanicek et al.

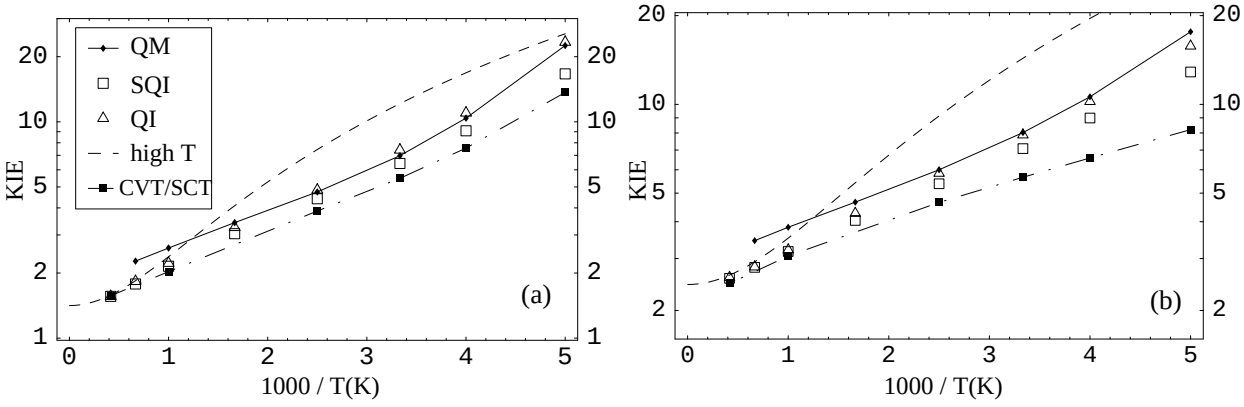

FIG. 5: J. Vanicek et al.